Ukrainian Journal of Physical Optics
ISSUE 2
2026

ANALYTICAL STUDY OF OPTICAL SOLITONS OF THE SPACE-TIME FRACTIONAL NONLINEAR SCHRÖDINGER EQUATIONS WITH KUDRYASHOV'S REFRACTIVE INDEX

WAEL W. MOHAMMED [1], MD. TIPU SULTAN [2], MOHAMED S. ALGOLAM [1], M. ALI AKBAR [3,4]* AND RABEB SIDAOUI [1]

[1] Department of Mathematics, College of Science, University of Ha'il, Ha'il 2440, Saudi Arabia
[2] Department of Applied Mathematics, Gono Bishwabidyalay, Savar, Dhaka, Bangladesh
[3] Miyan Research Institute, International University of Business Agriculture and Technology, Dhaka, Bangladesh
[4] Department of Applied Mathematics, University of Rajshahi, Bangladesh
*Corresponding Author: ali_math74@yahoo.com

Received: 02.02.2026

Abstract. In this article, we investigate the analytical optical solitons of two variants of the space-time fractional nonlinear Schrödinger equation, including Kudryashov's arbitrary refractive index. The models are formulated using the β-fractional derivative, which preserves the basic properties of classical calculus. The sine-Gordon expansion approach is used to originate exact and assorted soliton solutions, including complex, hyperbolic, and trigonometric forms. The obtained solutions describe a wide range of soliton structures, such as bright, dark, cuspon, kink, anti-kink, parabolic, and breather waves. A detailed parametric analysis shows that the fractional-order and nonlinear coefficients significantly affect the soliton amplitude, width, and propagation dynamics. The graphical simulations further confirm the stability and rich structural diversity of the solutions. The comparative results demonstrate that the sine-Gordon expansion approach is competent, accurate, and widely applicable. It also provides physically meaningful wave structures that are better than several existing techniques reported in the literature. The findings highlight the effectiveness of the proposed framework for modeling nonlinear pulse propagation in fractional optical fiber systems and related applications in nonlinear optics.

Keywords: Fractional nonlinear Schrödinger equation, β-fractional derivative, Sine-Gordon expansion approach, optical solitons, Kudryashov's refractive index
UDC: 517.958; 530.145; 517.955
DOI: 10.3116/16091833/Ukr.J.Phys.Opt.2026.02091
This work is licensed under the Creative Commons Attribution International License (CC BY 4.0).

1. Introduction

In recent times, there has been a significant increase in the study of the fractional nonlinear Schrödinger (NLS) model to investigate pulse propagation in optical fibers. Soliton theory has gained increasing importance in modern scientific research due to rapid progress in advanced science and technology. It is widely applied across physical disciplines, including nonlinear optics, optoelectronics, water waves, electrochemistry, image processing, probability, system identification, medicine, control theory, plasma physics, signal processing, and more [1-4]. Nonlinear optics, a well-established area of research, continues to attract significant attention from researchers worldwide. Fiber technology strongly drives progress in nonlinear optics and serves as an important foundation for communication engineering [5, 6]. Its significance in data transfer and communication has been growing exponentially. Kudryashov introduced an important nonlinear refractive index model in nonlinear optics [7]. This model explains the pulse propagation. The fractional nonlinear

Schrödinger equation (FNLSE) is a key tool for explicitly describing nonlinear models in optics. Accordingly, the FNLSE and their analytical soliton solutions are significant for understanding the complexities of physical phenomena and nonlinear optics [8]. Thus, several powerful methods are developed to obtain the optical soliton solutions for fractional and integer-order NLS equations, as for example the mapping method [9], the generalized Kudryashov method [10], the generalized Riccati equation technique [11], the sine-Gordon expansion approach [12], the Hirota bilinear approach [13], the modified Kudryashov scheme [14], the Sardar sub-equation process [15], the improved Bernoulli sub-equation function scheme [16], the (G'/G,1 / G)-expansion method [17], the modified extended direct algebraic process [18], etc.

After this, researchers developed different types of optical solitons for both classical and fractional NLS equations. They also used various analytical approaches to study the model's stability. Among them, Murad *et al*. [19] used the generalized exponential rational function scheme to analyze soliton behavior of a fractional dual-mode NLS model. Alraddadi *et al*. [20] derived soliton solutions to a (2+1)-dimensional classical generalized Korteweg-de Vries (KdV) equation through the generalized Riccati equation technique. Alam *et al*. [21] examined bifurcations, chaotic dynamics, and exact solutions to the fractional two-mode Nizhnik-Novikov-Veselov equation. Murad *et al*. [22] investigated new soliton patterns to the generalized derivative nonlinear conformable Schrödinger equation under multiplicative white-noise perturbations using the new Kudryashov approach. Samir *et al*. [23] explored bright, dark, and singular soliton structures of the (3+1)-dimensional Kadomtsev-Petviashvili equation through a modified extended direct algebraic methodology. Younas *et al*. [24] established parabolic, bright-dark, singular, and dark-singular soliton solutions to the Estévez-Mansfield-Clarkson equation by expanding the modified generalized exponential rational function method and the modified generalized Riccati equation mapping technique. Shehab *et al*. [25] derived singular, dark, and bright solitons of a stochastic nonlinear Schrödinger equation combining fourth-order perturbations. Ahmed *et al*. [26] applied an improved modified extended tanh-function scheme to the (3+1)-dimensional stochastic NLSE to investigate singular and composite dark-singular solitons. Samir *et al*. [27] obtained bright and dark solitons of a generalized stochastic NLSE exhibiting Brownian motion, quintic nonlinearity, and nonlinear chromatic dispersion using an improved modified extended tanh approach. In this article, we conduct a comprehensive analysis of optical solitons arising in two alternative versions of the NLS equation, with particular attention to the effects of Kudryashov's arbitrary refractive index and beta fractional derivative.

The fractional form of the space-time NLS equation with Kudryashov's arbitrary refractive index alongside two distinct nonlocal nonlinearities is considered as [28]:

$$iD_t^{\alpha}u + aD_{xx}^{2\alpha}u + \left(p_1|u|^n + p_2|u|^{2n} + p_3|u|^{3n} + p_4|u|^{4n}\right)u + \left(p_5D_{xx}^{2\alpha}|u|^n + p_6D_{xx}^{2\alpha}|u|^{2n}\right)u = 0, \qquad (1)$$

where $u(x,t)$ denotes the wave profile, and n represents the power nonlinearity. The coefficients p_k, k=1, 2, 3, and 4, correspond to higher-order self-phase modulation (SPM) effects, which describe intensity-dependent changes in the refractive index of the optical medium, and the coefficient a represents the velocity dispersion parameter, which controls the spreading or compression of optical pulses during propagation in a fiber. Furthermore,

the coefficients p_5 and p_6 quantify the strength of spatially nonlocal nonlinear refractive index contributions of orders n and $2n$, respectively. The operators D_t^{α} and $D_{xx}^{2\alpha}$ represent the beta fractional-order derivative (definition of beta fractional derivative and its properties are given in Section 2) with respect to time t and spatial coordinates x of order α and 2α, respectively, with $0<\alpha\le 1$.

Another variant of the time-space fractional form of the higher-order nonlinear Schrödinger equation is considered as [29, 30]:

$$iD_t^{\alpha}v + aD_{xx}^{2\alpha}v + \left(b_1|v|^n + b_2|v|^{2n} + \delta|v|^{3n} + b_3|v|^{4n} + b_4|v|^{5n} + \gamma|v|^{6n}\right)v = 0, \tag{2}$$

where $v(x,t)$ denotes the wave profile, n represents the power-law nonlinear exponent, and a is the dispersion coefficient. It controls the strength of the spatial dispersion term $D_{xx}^{2\alpha}v$, which manages how the wave spreads during propagation. b_1 is the coefficient of the first power nonlinearity $|v|^n v$, which represents the primary nonlinear response of the medium. b_2 is the coefficient of the second-order nonlinear term $|v|^{2n}v$; it introduces a higher-order nonlinear contribution that modifies the wave amplitude and stability. δ is the coefficient associated with the third-order nonlinear term $|v|^{3n}v$; it further strengthens nonlinear interactions in the system. b_3 is the coefficient of the fourth-order nonlinear term $|v|^{4n}v$, representing further higher-order nonlinear effects. b_4 is the coefficient of the fifth-order nonlinear term $|v|^{5n}v$, which contributes to stronger nonlinear modulation of the wave profile. γ is the coefficient of the sixth-order nonlinear term $|v|^{6n}v$, representing very high-order nonlinear effects that can influence the formation and stability of complex soliton structures. The operators D_t^{α} and $D_{xx}^{2\alpha}$ represent the beta fractional-order derivative with respect to time t and spatial coordinates x of order α and 2α.

Recently, various analytical methods have been developed by academics to obtain optical soliton solutions to Eq. (1); for example, Murad constructed bell-shaped, bright, and dark-bright solitons of this model using the Kudryashov approach [31]. Murad et al. acquired bell-shaped, bright, mixed dark-bright, and kink-type solitons of this model by putting in use the modified tanh expansion method [32]. Further, in [33], Murad et al. established the periodic, dark, bright, singular, bell-shaped, and mixed dark-bright solitons to the fractional Eq. (2) by using Bernoulli's equation approach. Elsherbeny et al. [11] used the extended auxiliary equation approach and modified Jacobi elliptic function scheme to obtain exact solitary wave solutions. Elsayed et al. [34] exploited the new mapping scheme and the unified Riccati equation method to construct soliton solutions. Biswas et al. applied the semi-inverse variational principle [35] to retrieve soliton solutions in two nonlinear models of the refractive index. In [36], Ozisik et al. constructed soliton solutions using the direct mapping method. Xu employed the trial equation method and the complete discriminant system for the polynomial method [37] to exact chirped solutions for the above model (1). The first model (1) generalizes the NLS equation through the inclusion of the Kudryashov variable refractive index and two distinct nonlocal nonlinearities, while the second model (2) focuses narrowly on soliton pulse propagation in optical fiber systems. Essentially, the fractional NLSE enhanced by Kudryashov's arbitrary refractive index and two types of nonlocal

nonlinearities signifies an important advance in nonlinear optics, providing greater adaptability, more pronounced nonlinear behavior, new soliton families, and stronger predictive performance than the classical NLSE version. Studying the time-fractional nonlinear Schrödinger equation is important both scientifically and practically. It includes Kudryashov's arbitrary refractive index and two types of nonlocal nonlinearities. This helps us understand complex wave propagation processes in media exhibiting fractional-time behavior and nonlocal effects.

Prior studies have employed various analytical schemes, such as the Kudryashov, Bernoulli, and Jacobi elliptic function methods, to obtain optical soliton solutions of the fractional- and integer-order nonlinear Schrödinger equations. However, the model Eq's. (1) and (2) within the combined framework of the generalized Kudryashov nonlinear refractive index and the beta-fractional derivative, using the sine-Gordon expansion (SGE) approach, have not been investigated. Consequently, the effects of fractional parameters and nonlocal nonlinearities on soliton behavior have not been appropriately examined. Therefore, the present study aims to bridge this gap by employing the SGE technique [38] to derive broad, stable, and exact optical soliton solutions expressed in complex, hyperbolic, and trigonometric forms for two variants of the fractional NLS model. The objective also includes examining how fractional parameters affect soliton amplitude, width, and propagation. This study further examines the efficiency, effectiveness, and general applicability of the SGE approach in solving fractional nonlinear evolution equations relevant to optical fiber communication and applied physics.

The article is organized as follows: Section 2 presents the definition and properties of the beta fractional derivative framework. Section 3 presents the sine-Gordon expansion technique. In Section 4, this method is applied to investigate Kudryashov's generalized fractional nonlinear Schrödinger models of refractive index. Section 5 provides the graphical interpretations of the results. In Section 6, we discussed solutions for integer- and fractional-order modeling. In Section 7, we delineate the stability analysis of the considered model, and Section 8 concludes with final remarks and observations.

2. The beta derivative

Many researchers proposed the definition of fractional-order derivative [39-41]. Most of them do not follow the derivative of a constant is zero, the chain rule, and the Leibnitz rule. Recently, Atangana *et al*. [42] presented an advanced and significant definition of the fractional derivative called the β derivative. This definition behaves well and fulfills all the properties of classical calculus, including the chain and Leibniz rules [42]. The β-fractional derivative is further flexible in describing effects that the classical derivative cannot represent.

The β-derivative is more appropriate than standard fractional operators in physical situations where the system exhibits fractional-order scaling or stretched dynamics but does not involve long-term memory effects. In such cases, the irregularity in the system arises mainly from local structural complexity or scaling properties rather than nonlocal temporal impact. Instances include local diffusion or transport in heterogeneous or porous media, where anomalous behavior arises from geometric complexity. The β-derivative is applied to nonlinear wave phenomena, such as optical solitons and ion-acoustic waves, and to equations like the modified KdV-KP model. It is also useful in epidemiological and biological

population models, such as the spread of dengue, Ebola, or rubella. In these models, the β-derivative introduces an additional scaling parameter that improves data fitting while keeping the model mathematically simple. In chaotic dynamical systems and boundary-layer problems, the β-derivative preserves the classical rules of calculus. This allows conventional stability analysis, Lyapunov exponent evaluation, and the direct application of classical initial conditions. Thus, the β-derivative is useful as a flexible scaling mechanism for fractional-order modeling when nonlocality or memory effects are weak. Therefore, in this study, we consider the β-fractional derivative to model the space-time fractional higher-order nonlinear Schrödinger equation.

Definition: Let $a\epsilon\ \mathbb{R}$ and u be function such that $u:[a,\infty)\to\mathbb{R}$. Then the λ-order derivate of u is defined as [43]:

$$D_y^{\lambda}u(y)=\lim_{\varepsilon\to 0}\frac{u\left(y+\varepsilon\left(y+\frac{1}{\Gamma(\lambda)}\right)^{1-\lambda}\right)-u(y)}{\varepsilon},\ y\geq 0,\ 0<\lambda\leq 1,$$ and Γ is the gamma function.

From the above definition, we have $D_y^{\lambda}u(y)=\frac{d}{dy}u(y)$, for $\lambda=1$.

Properties of beta derivative: Consider $f(y)$ and $h(y)$ are λ-order differentiable for all $y>0$ and if b and c are real constants, then the subsequent rules are satisfied [44] by this definition: $D_y^0 f(y)=f(y)$, $D_y^{\lambda}\left(bf(y)+ch(y)\right)=bD_y^{\lambda}\left(f(y)\right)+cD_y^{\lambda}\left(h(y)\right)$, $D_y^{\lambda}\left(f(y)h(y)\right)=f(y)D_y^{\lambda}\left(h(y)\right)+h(y)D_y^{\lambda}\left(f(y)\right)$, $D_y^{\lambda}\left(f^{-1}(y)\right)=-\left[D_y^{\lambda}\left(f(y)\right)/f^2(y)\right]$, $D_y^{\lambda}\left(\frac{f(y)}{h(y)}\right)=\left(h(y)D_y^{\lambda}\left(f(y)\right)-f(y)D_y^{\lambda}\left(h(y)\right)\right)/h^2(y)$, $D_y^{\lambda}\left((foh)(y)\right)=D_y^{\lambda}\left(f\left(h(y)\right)\right)h'(y)$, $D_y^{\lambda}\left(f(y)\right)=\left(y+\frac{1}{\Gamma(\lambda)}\right)^{1-\lambda}\frac{df(y)}{dy}$. Because of its usefulness, simplicity, and accessibility, many academics have employed this notable definition of the fractional derivative in numerous physical applications [44, 45].

The physical significance and limitations of the β-derivative: The β-derivative is a generalized differential operator that extends classical derivatives to fractional orders. It preserves standard calculus rules, including the chain rule and product rule. It models systems with fractional-order scaling or stretched dynamics, capturing intermediate behaviors between integer-order dynamics without assuming long-term memory effects. Despite its usefulness, the β-derivative has some limitations. It cannot model history-dependent or nonlocal phenomena, so it is unsuitable for systems where memory effects and long-term correlations are significant. Additionally, the choice of the β parameter is often empirical, which can reduce predictive accuracy in practical applications. Although it follows the classical calculus rules, the β-derivative cannot describe all types of anomalous diffusion, viscoelasticity, or other complex behaviors that standard fractional derivatives can.

3. The sine-Gordon expansion approach

In this section, we discuss the sine-Gordon expansion (SGE) approach in detail. The SGE approach is a more flexible and efficient method that provides a more unified and systematic

framework compared to the latest reported approaches, such as the Bernoulli equation method, Hirota method, sine-cosine method, and exp-function method. Unlike these techniques, the suggested method can generate numerous soliton profiles within a single procedure while accurately capturing both dissipative and dispersive nonlinearities in the nonlinear Schrödinger equations under Kudryashov's arbitrary refractive index. It can handle complex algebraic expressions and generate meaningful, structurally diverse solution forms. This makes it a stronger and more flexible method for studying nonlinear evolution equations. These advantages highlight its improved effectiveness over existing methods. The SGE method is demonstrated as follows.

Let us consider the standard form of the sine-Gordon fractional equation of two variables, x and t, as follows [12, 38]:

$$\mathcal{D}_x^{2\delta} f - \mathcal{D}_t^{2\delta} f = A^2 \sin(f), \tag{3}$$

where A is a constant, and $\mathcal{D}_x^{2\delta}$, $\mathcal{D}_t^{2\delta}$ represents the fractional 2δ - order derivative with respect to x and t, respectively. The suitable fractional form of the function $f(x,t) = F(\xi)$ with $\xi = \frac{a}{\delta}\left(x + \frac{1}{\Gamma(\delta)}\right)^{\delta} + \frac{c}{\delta}\left(t + \frac{1}{\Gamma(\delta)}\right)^{\delta}$, under the wave transformation, converts the fractional sine-Gordon equation into a one-dimensional form in the following form

$$\frac{d^2F}{d\xi^2} = \frac{A^2}{a^2 - c^2}\sin(F), \tag{4}$$

where c is the speed of the travelling wave. Some simplification leads to the following equation

$$\left(\frac{d}{d\xi}\left(\frac{F}{2}\right)\right)^2 = \frac{A^2}{a^2 - c^2}\sin^2\left(\frac{F}{2}\right) + k, \tag{5}$$

where k is a constant of integration. For simplicity, let us assume that $k = 0$, $Y(\xi) = F(\xi)/2$, and $\frac{A^2}{a^2 - c^2} = 1$. Then Eq. (5) is converted to

$$\frac{dY}{d\xi} = \sin(Y(\xi)). \tag{6}$$

Eq. (6) gives the following relations

$$\sin(Y(\xi)) = \frac{2pe^{\xi}}{p^2e^{2\xi} + 1} = \operatorname{sech}(\xi), \tag{7}$$

or

$$\cos(Y(\xi)) = \frac{p^2e^{2\xi} - 1}{p^2e^{2\xi} + 1} = \tanh(\xi), \tag{8}$$

where p is a non-zero integral constant. The conformable fractional differential equation

$$g(f, \mathcal{D}_t^{\delta} f, \mathcal{D}_x^{\delta} f, \mathcal{D}_{tt}^{2\delta} f, \mathcal{D}_{xx}^{2\delta} f, \mathcal{D}_{xt}^{2\delta} f, \ldots) = 0, \tag{9}$$

can be reduced to the subsequent nonlinear equation of one variable

$$\hat{g}(F, F', F'', F''', \ldots) = 0, \tag{10}$$

by using a suitable wave variation $f(x,t) = F(\xi)$, where the changing variable ξ is defined

as $\xi = \frac{a}{\delta}\left(x + \frac{1}{\Gamma(\delta)}\right)^{\delta} + \frac{c}{\delta}\left(t + \frac{1}{\Gamma(\delta)}\right)^{\delta}$. Symbols such as F', F'', F''',... are used to represent the successive derivatives of F, namely $\frac{dF}{d\xi}$, $\frac{d^2F}{d\xi^2}$, $\frac{d^3F}{d\xi^3}$, and so on.

In the sine-Gordon expansion approach, the solutions of Eq. (10) are considered in the following form

$$F(\xi) = A_0 + \sum_{j=1}^{N} \tanh^{j-1}(\xi)\left(B_j \operatorname{sech}(\xi) + A_j \tanh(\xi)\right). \tag{11}$$

By means of (7) and (8), solution (11) can be written as

$$F(Y) = A_0 + \sum_{j=1}^{N} \cos^{j-1}(Y)\left(B_j \sin(Y) + A_j \cos(Y)\right). \tag{12}$$

The positive integer N in Eq. (12) can be determined by taking into consideration the homogeneous balance between the highest-order derivative and the highest-order nonlinear terms arising in equation (10). Substituting the predicted solution (12) into (10) and taking the coefficients of like powers of $\sin^i(Y)$ and $\cos^j(Y)$ as zero, we get the system of algebraic equations. Solving this system of equations, we acquire the values of A_0, A_1, A_2, B_1, B_2,..., a, and c. Then, the required solutions, if they exist, are obtained using equations (11), (12), and ξ. The limitations and advantages of the methods are provided in Table 1 below.

Table 1. The limitations and the advantages of the methods.

Method	Advantages	Limitations
The Bernoulli equation approach	Distinguished by its simplicity and speed, it enables direct construction of explicit solutions containing free parameters.	Its methodological rigidity restricts the variety of obtainable solutions, making it inadequate for capturing intricate nonlinear behaviors or solving many types of partial differential equations.
The sine-Gordon expansion approach	Particularly useful for producing oscillatory, periodic, and kink-like waveforms due to its versatile mathematical formulation.	The method requires substantial algebraic work and relies on the PDE's inherent compatibility with the sine-Gordon expansion structure.

4. Extraction of solutions

The aim of this module is to attain the general, comprehensive, and stable soliton solutions of two different forms of the NLS equation in the presence of Kudryashov's arbitrary refractive index model using the SGE approach, from which some known optical soliton solutions can be extracted.

4.1. The fractional space-time NLS equation

Assume the solution of Eq. (1) has the traveling wave solution of the form

$$u(x,t) = U(\xi)e^{i\theta}. \tag{13}$$

The wave variables ξ and θ are defined by

$$\begin{aligned} \xi &= \frac{1}{\alpha}\left(x + \frac{1}{\Gamma(\alpha)}\right)^{\alpha} - \frac{v}{\alpha}\left(t + \frac{1}{\Gamma(\alpha)}\right)^{\alpha} \\ \text{and} \quad \theta &= l - \frac{k}{\alpha}\left(x + \frac{1}{\Gamma(\alpha)}\right)^{\alpha} + \frac{\omega}{\alpha}\left(t + \frac{1}{\Gamma(\alpha)}\right)^{\alpha} \end{aligned} \tag{14}$$

where v, ω, k, and l are the wave velocity, soliton frequency, wave number, and phase constant, respectively. Using (13) and (14) in Eq. (1) and then upon simplification, the imaginary part of the equation can be written as

$$U'\left(v+2ak\right)=0. \tag{15}$$

Since we are looking for nontrivial travelling wave solutions, the condition $U'=0$ would imply that U is a constant, which corresponds to a trivial and physically unrealistic solution. Therefore, to obtain meaningful travelling wave profiles, we require $U'\neq 0$. Therefore, from Eq. (15), we get

$$v=-2ak, \tag{16}$$

which gives the velocity of the travelling wave.

The real part of the equation is given by

$$\begin{aligned} &aU''-U\left(\omega+ak^2\right)+2np_6U''U^{2n}+np_5U''U^n+2np_6\left(2n-1\right)U^{2n-1}\left(U'\right)^2 \\ &+p_5n\left(n-1\right)U^{n-1}\left(U'\right)^2+p_1U^{n+1}+p_2U^{1+2n}+p_3U^{1+3n}+p_4U^{1+4n}=0. \end{aligned} \tag{17}$$

From Eq. (17), the balancing principle yields $N=1/n$. Therefore, we assume the transformation

$$U\left(\xi\right)=\phi\left(\xi\right)^{\frac{1}{n}}. \tag{18}$$

The transformation $U=\phi^{1/n}$ requires $\phi>0$ if the exponent $1/n$ is not an integer or the context demands real-valued outputs. If n is an odd integer, the transformation is defined for all real ϕ, but the equation assumes $\phi>0$ so that the expression is clearly real for any y n. Thus, the domain restriction is $\phi>0$ unless otherwise specified for an odd integer n. By using (18), Eq. (17) can be written as

$$\begin{aligned} &an\phi\phi''+a\left(1-n\right)\left(\phi'\right)^2+p_5n^2\phi^3\phi''+p_5n\left(1-n\right)\phi^2\left(\phi'\right)^2+2p_6n^2\phi^3\phi'' \\ &+2p_6n\left(1-n\right)\phi^2\left(\phi'\right)^2-n^2\left(ak^2+\omega\right)\phi^2+p_1n^2\phi^3+p_2n^2\phi^4+p_3n^2\phi^5+p_4n^2\phi^6=0. \end{aligned} \tag{19}$$

The balancing principle between ϕ^6, and $\phi''\phi^3$ in Eq. (19) gives $6N=4N+2$ and thus we find $N=1$. Therefore, the solution of Eq. (19) takes the following form

$$\phi\left(\xi\right)=A_0+B_1\sin\left(Y\right)+A_1\cos\left(Y\right). \tag{20}$$

By substituting Eq. (20) into Eq. (19), then simplifying and equating the coefficients of like powers of $\sin\left(Y\right)$ and $\cos\left(Y\right)$ on both sides, we obtained some algebraic system of equations. After unraveling this algebraic system of equations with the help of Maple, we have obtained the following set of solutions:

Set 1:

$$\begin{aligned} &A_0=0, A_1=0, B_1=\pm\sqrt{\frac{6p_6}{p_4}}, p_1=-p_5 \\ &p_2=\frac{-24n^2p_6^2+anp_4+ap_4}{6n^2p_6}, p_3=\frac{p_4p_5}{3p_6}, \omega=-\frac{a\left(k^2n^2-1\right)}{n^2} \end{aligned}, \tag{21}$$

where a and k are arbitrary parameters with $p_6\neq 0$, $p_4\neq 0$, and $n\neq 0$. Substituting the values of the parameter from (21) into solution (20), along with (13), (14), and (18), the soliton solution of the fractional space-time NLS model is as follows:

$$u_1(x,t)=\pm\left(\frac{6p_6}{p_4}\right)^{1/n}\operatorname{sech}^{1/n}(\xi)\times\exp\left[i\left(l-\frac{k}{\alpha}\left(x+\frac{1}{\Gamma(\alpha)}\right)^{\alpha}+\frac{\left(-\frac{a(k^2n^2-1)}{n^2}\right)}{\alpha}\left(t+\frac{1}{\Gamma(\alpha)}\right)^{\alpha}\right)\right], \tag{22}$$

where $\xi=\frac{1}{\alpha}\left(x+\frac{1}{\Gamma(\alpha)}\right)^{\alpha}+\frac{2ak}{\alpha}\left(t+\frac{1}{\Gamma(\alpha)}\right)^{\alpha}$.

Set 2:

$$A_0=\sqrt{-\frac{6p_6}{p_4}},\ p_1=-\frac{an\sqrt{-\frac{6p_6}{p_4}}p_4+12n^2p_6p_5+2a\sqrt{-\frac{6p_6}{p_4}}p_4}{3n^2p_6},\ p_3=-\frac{p_4\left(10p_6\sqrt{-\frac{6p_6}{p_4}}-p_5\right)}{3p_6},$$
$$A_1=\pm\sqrt{-\frac{6p_6}{p_4}},\omega=-\frac{a(k^2n^2-4)}{n^2},B_1=0,p_2=-\frac{6n^2\sqrt{-\frac{6p_6}{p_4}}p_5p_4+96n^2p_6^2-anp_4-ap_4}{6n^2p_6} \tag{23}$$

By inserting the values of the parameter presented in (23) into the solution given in (20), and utilizing the relations defined in (13), (14), and (18), we derive the corresponding soliton solution for the fractional space-time NS model. This substitution process yields an explicit analytical expression that characterizes the soliton structure and captures the essential nonlinear dynamics of the proposed fractional model.

$$u_2(x,t)=\left(\sqrt{-\frac{6p_6}{p_4}}\pm\sqrt{-\frac{6p_6}{p_4}}\tanh(\xi)\right)^{\frac{1}{n}}\times\exp\left[i\left(l-\frac{k}{\alpha}\left(x+\frac{1}{\Gamma(\alpha)}\right)^{\alpha}+\frac{\left(-\frac{a(k^2n^2-4)}{n^2}\right)}{\alpha}\left(t+\frac{1}{\Gamma(\alpha)}\right)^{\alpha}\right)\right], \tag{24}$$

The expression $\sqrt{-6p_6/p_4}$ must be real; thus, the parameters must satisfy the restriction $-6p_6/p_4>0$, which implies that p_6 and p_4 must have opposite signs with $p_4\neq 0$.

Set 3:

$$p_1=-\frac{-an\sqrt{-\frac{6p_6}{p_4}}p_4+12n^2p_6p_5-2a\sqrt{-\frac{6p_6}{p_4}}p_4}{3n^2p_6},\ p_3=-\frac{p_4\left(-10p_6\sqrt{-\frac{6p_6}{p_4}}-p_5\right)}{3p_6},$$
$$A_0=-\sqrt{-\frac{6p_6}{p_4}},A_1=\pm\sqrt{-\frac{6p_6}{p_4}},p_2=-\frac{-6n^2\sqrt{-\frac{6p_6}{p_4}}p_5p_4+96n^2p_6^2+anp_4+ap_4}{6n^2p_6}, \tag{25}$$
$$B_1=0,\omega=-\frac{a(k^2n^2-4)}{n^2}.$$

By substituting the parameter values specified in Eq. (25) into the general solution (20) and employing the relations defined in (13), (14), and (18), the corresponding soliton solution for the fractional space-time NS model is obtained.

$$u_3(x,t)=\left(-\sqrt{-\frac{6p_6}{p_4}}\pm\sqrt{-\frac{6p_6}{p_4}}\tanh(\xi)\right)^{\frac{1}{n}} \times\exp\left[i\left(l-\frac{k}{\alpha}\left(x+\frac{1}{\Gamma(\alpha)}\right)^{\alpha}+\frac{\left(-\frac{a(k^2n^2-4)}{n^2}\right)}{\alpha}\left(t+\frac{1}{\Gamma(\alpha)}\right)^{\alpha}\right)\right], \tag{26}$$

Set 4:

$$A_0=\sqrt{-\frac{3p_6}{2p_4}},\ A_1=\pm\sqrt{-\frac{3p_6}{2p_4}},\ B_1=\sqrt{3p_6/2p_4},\ p_1=-\frac{2n^2p_5\sqrt{-\frac{3p_6}{2p_4}}-an-2a}{2n^2\sqrt{-\frac{3p_6}{2p_4}}},$$

$$p_2=-\frac{6n^2p_5\sqrt{-\frac{3p_6}{2p_4}}p_4+24n^2p_6^2-anp_4-ap_4}{6n^2p_6},\ p_3=\frac{p_5p_4\sqrt{-\frac{3p_6}{2p_4}}+15p_6^2}{3p_6\sqrt{-\frac{3p_6}{2p_4}}}, \tag{27}$$

$$\omega=-\frac{a(k^2n^2-1)}{n^2},$$

By substituting the parameter values specified in (27) into the solution (20) and applying the relations defined in (13), (14), and (18), the corresponding soliton solution for the fractional space-time NLS model is derived. This substitution provides an explicit analytical form of the soliton and reveals how the fractional parameters influence the wave structure, amplitude, and propagation characteristics.

$$u_4(x,t)=\left(\sqrt{-\frac{3p_6}{2p_4}}+\frac{\sqrt{\frac{6p_6}{p_4}}}{2}\operatorname{sech}(\xi)\pm\sqrt{-\frac{3p_6}{2p_4}}\tanh(\xi)\right)^{\frac{1}{n}} \times\exp\left[i\left(l-\frac{k}{\alpha}\left(x+\frac{1}{\Gamma(\alpha)}\right)^{\alpha}-\left(\frac{a(k^2n^2-1)}{\alpha n^2}\right)\left(t+\frac{1}{\Gamma(\alpha)}\right)^{\alpha}\right)\right], \tag{28}$$

where $\xi=\frac{1}{\alpha}\left(x+\frac{1}{\Gamma(\alpha)}\right)^{\alpha}+\frac{\omega}{\alpha}\left(t+\frac{1}{\Gamma(\alpha)}\right)^{\alpha}$.

Set 5:

$$A_0=-\sqrt{-\frac{3p_6}{2p_4}},\ A_1=\pm\sqrt{-\frac{3p_6}{2p_4}},\ B_1=\frac{\sqrt{\frac{6p_6}{p_4}}}{2},\ p_2=-\frac{-6n^2p_5\sqrt{-\frac{3p_6}{2p_4}}p_4+24n^2p_6^2-anp_4-ap_4}{6n^2p_6},$$

$$p_1=\frac{-2n^2p_5\sqrt{-\frac{3p_6}{2p_4}}-an-2a}{2n^2\sqrt{-\frac{3p_6}{2p_4}}},\ \omega=-\frac{a(k^2n^2-1)}{n^2},\ p_3=-\frac{-p_5p_4\sqrt{-\frac{3p_6}{2p_4}}+15p_6^2}{3p_6\sqrt{-\frac{3p_6}{2p_4}}}, \tag{29}$$

By inserting the parameter values from (29) into solution (20) and using the relations in (13), (14), and (18), the soliton solution of the fractional space-time NLS model is obtained, which may reveal the effect of fractional parameters on the wave's structure, amplitude, and propagation.

$$u_5(x,t)=\left(-\sqrt{-\frac{3p_6}{2p_4}}+\sqrt{\frac{3p_6}{2p_4}}\operatorname{sech}(\xi)\pm\sqrt{-\frac{3p_6}{2p_4}}\tanh(\xi)\right)^{\frac{1}{n}} \times\exp\left[i\left(l-\frac{k}{\alpha}\left(x+\frac{1}{\Gamma(\alpha)}\right)^{\alpha}+\frac{\left(-\frac{a(k^2n^2-1)}{n^2}\right)}{\alpha}\left(t+\frac{1}{\Gamma(\alpha)}\right)^{\alpha}\right)\right], \tag{30}$$

Set 6:

$$A_0=\sqrt{-\frac{3p_6}{2p_4}},\ A_1=\pm\sqrt{-\frac{3p_6}{2p_4}},\ B_1=-\sqrt{\frac{3p_6}{2p_4}},\ p_1=-\frac{2n^2p_5\sqrt{-\frac{3p_6}{2p_4}}-an-2a}{2n^2\sqrt{-\frac{3p_6}{2p_4}}},$$

$$p_2=-\frac{6n^2p_5\sqrt{-\frac{3p_6}{2p_4}}p_4+24n^2p_6^2-anp_4-ap_4}{6n^2p_6},\ p_3=\frac{p_5p_4\sqrt{-\frac{3p_6}{2p_4}}+15p_6^2}{3p_6\sqrt{-\frac{3p_6}{2p_4}}}, \tag{31}$$

$$\omega=-\left(a\left(k^2n^2-1\right)\right)/n^2,$$

By setting the parameter values provided in Eq. (31) into the general form of solution (20) and employing the auxiliary relations defined in (13), (14), and (18), the analytical soliton solution corresponding to the fractional space-time NLS model is constructed. This formulation highlights the significant role of fractional parameters in modulating the soliton's structural profile, amplitude behavior, and propagation dynamics within the nonlinear medium.

$$u_6(x,t)=\left(\sqrt{-\frac{3p_6}{2p_4}}-\sqrt{\frac{3p_6}{2p_4}}\operatorname{sech}(\xi)\pm\sqrt{-\frac{3p_6}{2p_4}}\tanh(\xi)\right)^{\frac{1}{n}} \times\exp\left[i\left(l-\frac{k}{\alpha}\left(x+\frac{1}{\Gamma(\alpha)}\right)^{\alpha}+\frac{\left(-\frac{a(k^2n^2-1)}{n^2}\right)}{\alpha}\left(t+\frac{1}{\Gamma(\alpha)}\right)^{\alpha}\right)\right], \tag{32}$$

Set 7:

$$A_0=-\sqrt{-\frac{3p_6}{2p_4}},\ A_1=\pm\sqrt{-\frac{3p_6}{2p_4}},\ B_1=-\sqrt{\frac{3p_6}{2p_4}},\ p_1=\frac{-2n^2p_5\sqrt{-\frac{3p_6}{2p_4}}-an-2a}{2n^2\sqrt{-\frac{3p_6}{2p_4}}},$$

$$p_2=-\frac{-6n^2p_5\sqrt{-\frac{3p_6}{2p_4}}p_4+24n^2p_6^2-anp_4-ap_4}{6n^2p_6},\ p_3=-\frac{-p_5p_4\sqrt{-\frac{3p_6}{2p_4}}+15p_6^2}{3p_6\sqrt{-\frac{3p_6}{2p_4}}}, \tag{33}$$

$$\omega=-\frac{a\left(k^2n^2-1\right)}{n^2},$$

By putting the parameter values from (33) to solution (20) and using the relations in (13), (14), and (18), the analytical soliton solution of the fractional space-time NLS model is obtained, demonstrating how fractional parameters govern the soliton's shape, amplitude, and propagation in the nonlinear medium.

$$u_7(x,t)=\left(-\sqrt{-\frac{3p_6}{2p_4}}-\sqrt{\frac{3p_6}{2p_4}}\operatorname{sech}(\xi)\pm\sqrt{-\frac{3p_6}{2p_4}}\tanh(\xi)\right)^{\frac{1}{n}} \times\exp\left[i\left(l-\frac{k}{\alpha}\left(x+\frac{1}{\Gamma(\alpha)}\right)^{\alpha}+\frac{\left(-\frac{a(k^2n^2-1)}{n^2}\right)}{\alpha}\left(t+\frac{1}{\Gamma(\alpha)}\right)^{\alpha}\right)\right], \tag{34}$$

The variation of free parameters yields a comfortable and further intricate assortment of solution structures for the refractive generalized form of Kudryashov's fractional nonlinear Schrödinger equation. These outcomes are excluded from this analysis to maintain brevity.

4.2. The time-space fractional higher-order NLS equation

We assumed the solution of Eq. (2) is of the form

$$v(x,t)=V(\xi)e^{i\eta}. \tag{35}$$

The wave variables ξ and η are defined by

$$\xi=\frac{1}{\alpha}\left(x+\frac{1}{\Gamma(\alpha)}\right)^{\alpha}-\frac{c}{\alpha}\left(t+\frac{1}{\Gamma(\alpha)}\right)^{\alpha}$$

and , (36)

$$\eta=-\frac{k}{\alpha}\left(x+\frac{1}{\Gamma(\alpha)}\right)^{\alpha}+\frac{\omega}{\alpha}\left(t+\frac{1}{\Gamma(\alpha)}\right)^{\alpha},$$

where c, ω, and k are the wave speed, wave frequency, and wave number of the soliton, respectively. By using the definition of beta fractional derivative with Eq's. (35) and (36) in Eq. (2), and then simplifying, the imaginary and real parts of the equation can be written as

$$V'(c+2ak)=0. \tag{37}$$

In Eq. (37), we assume $V'\neq 0$, because the aim is to construct nontrivial traveling wave solutions. If $V'=0$, then V reduces to a constant function. Such constant solutions do not represent traveling waves and correspond to trivial equilibrium states of the model, offering no wave structure or physical propagation. Since the analysis focuses on meaningful travelling-wave profiles with spatio-temporal variation, constant solutions are excluded here. Therefore, $V'\neq 0$ yields

$$c=-2ak, \tag{38}$$

which gives the velocity of the travelling wave. The real part of the equation is given by

$$aV''-V(\omega+ak^2)+b_1V^{n+1}+b_2V^{1+2n} +\delta V^{1+3n}+b_3V^{1+4n}+b_4V^{1+5n}+\gamma V^{1+6n}=0. \tag{39}$$

For an integer balancing number, we consider the transformation

$$V(\xi)=U(\xi)^{\frac{1}{3n}}. \tag{40}$$

By using Eq. (40), Eq. (39) can be written as

$$3anU^{\left(\frac{1}{3n}-1\right)}U''+a(1-3n)U^{\left(\frac{1}{3n}-2\right)}(U')^2+9b_1n^2U^{\left(\frac{1}{3n}+1\right)}+9b_2n^2U^{\left(\frac{1}{3n}+2\right)}+9\delta n^2U^{\left(\frac{1}{3n}+1\right)} +9b_3n^2U^{\frac{1+4n}{3n}}+9b_4n^2U^{\frac{1+5n}{3n}}+9\gamma n^2U^{\left(\frac{1}{(3n}+2\right)}-9n^2(\omega+ak^2)U^{\frac{1}{3n}}=0. \tag{41}$$

For the integrability of Eq. (41), we set $b_1 = b_2 = b_3 = b_4 = 0$, and then it is attained

$$3anU^{\left(\frac{1}{3n}-1\right)}U'' + a(1-3n)U^{\left(\frac{1}{3n}-2\right)}(U')^2 + 9\delta n^2 U^{\left(\frac{1}{3n}+1\right)} + 9\gamma n^2 U^{\left(\frac{1}{(3n}+2\right)} - 9n^2(\omega + ak^2)U^{\frac{1}{3n}} = 0$$

Multiplying the above equation by $U^{\frac{-1}{3n}}U^2$ and simplifying, we obtain

$$3anUU'' + a(1-3n)(U')^2 + 9n^2\delta U^3 + 9n^2\gamma U^4 - 9n^2(ak^2 + \omega)U^2 = 0. \quad (42)$$

The balancing principle between U^4 and UU'', it gives $4N = 2N + 2$, and thus we find $N = 1$. Now, the solution of Eq. (42) takes the following form

$$U(\xi) = A_0 + B_1 \sin(Y) + A_1 \cos(Y). \quad (43)$$

By substituting Eq. (43) into Eq. (42), then simplifying and equating the coefficients of like powers of $\sin^i(Y)$ and $\cos^j(Y)$ on both sides, we obtained an algebraic system of equations. After solving this algebraic system of equations with the help of Maple, we have obtained the following set of solutions:

Set 1:

$$A_0 = \pm\frac{\sqrt{-\frac{3an+a}{9\gamma}}}{n}, A_1 = \pm\frac{\sqrt{-\frac{3an+a}{9\gamma}}}{n}, B_1 = 0, \omega = -\frac{a(9n^2k^2-4)}{9n^2}, \delta = \pm\frac{2a(3n+2)}{9n\sqrt{-\frac{3an+a}{9\gamma}}}, \quad (44)$$

where a and k are arbitrary parameters with $\gamma \neq 0$, $n \neq 0$. By substituting the values of the parameter from (44) into solution (43) and applying the relations in (35), (36), and (40), the analytical soliton solution of the fractional space-time NLS model is derived. This shows the effect of fractional parameters on the soliton's shape, amplitude, and propagation in the nonlinear medium.

$$v_1(x,t) = \left(\pm\frac{\sqrt{-\frac{3an+a}{9\gamma}}}{n} \pm \frac{\sqrt{-\frac{3an+a}{9\gamma}}}{n}\tanh(\xi)\right)^{\frac{1}{3n}} \times \exp\left[i\left(-\frac{k}{\alpha}\left(x+\frac{1}{\Gamma(\alpha)}\right)^{\alpha} + \frac{\left(-\frac{(9n^2k^2-4)a}{9n^2}\right)}{\alpha}\left(t+\frac{1}{\Gamma(\alpha)}\right)^{\alpha}\right)\right], \quad (45)$$

where $\xi = \frac{1}{\alpha}\left(x+\frac{1}{\Gamma(\alpha)}\right)^{\alpha} + \frac{2ak}{\alpha}\left(t+\frac{1}{\Gamma(\alpha)}\right)^{\alpha}$.

Set 2:

$$A_0 = \pm\frac{\sqrt{\frac{-3an-a}{36\gamma}}}{n}, A_1 = \pm\frac{\sqrt{-\frac{3an+a}{36\gamma}}}{n}, B_1 = \pm\frac{\sqrt{\frac{3an+a}{36\gamma}}}{n}, \omega = -\frac{(9n^2k^2-1)a}{9n^2}, \delta = \pm\frac{(3n+2)a}{18n\sqrt{\frac{-3an-a}{36\gamma}}}, \quad (46)$$

where a and k are arbitrary parameters with $\gamma \neq 0$, $n \neq 0$, and $\frac{-3an-a}{36\gamma} > 0$. Inserting the values of the parameter from (46) into solution (43) and using the relations in (35), (36), and (40), the analytical soliton solution of the fractional space-time NLS model is achieved. This illustrates the impact of fractional parameters on the soliton's shape, amplitude, and propagation of the wave.

$$v_2(x,t) = \left(\pm\frac{\sqrt{-\frac{3an+a}{36\gamma}}}{n} \pm \frac{\sqrt{\frac{3an+a}{36\gamma}}}{n}\operatorname{sech}(\xi) \pm \frac{\sqrt{-\frac{3an+a}{36\gamma}}}{n}\tanh(\xi) \right)^{\frac{1}{3n}} \times \exp\left\{ i\left(-\frac{k}{\alpha}\left(x + \frac{1}{\Gamma(\alpha)} \right)^{\alpha} + \frac{\left(-\frac{(9n^2k^2-1)a}{9n^2} \right)}{\alpha}\left(t + \frac{1}{\Gamma(\alpha)} \right)^{\alpha} \right) \right\}, \tag{47}$$

Exploration of different values for the free parameters reveals a significantly more elaborate set of solution structures for the fractional nonlinear Schrödinger equation. However, these findings are omitted here for conciseness.

5. Characteristics of the solutions and explanation

In this section, we will discuss the graphical representation of the obtained analytical solutions for different values of the variables. We draw the graph of these solutions by using the symbolic computation tool Mathematica.

5.1. The space-time fractional NLS equation

In this section, we describe the graphical representations of the solutions obtained for the space-time fractional NLS equation with Kudryashov's arbitrary refractive index, alongside two distinct nonlocal nonlinear models for different parameter values. The 3-dimensional, 2-dimensional, density, and contour plots of the solutions obtained are provided below.

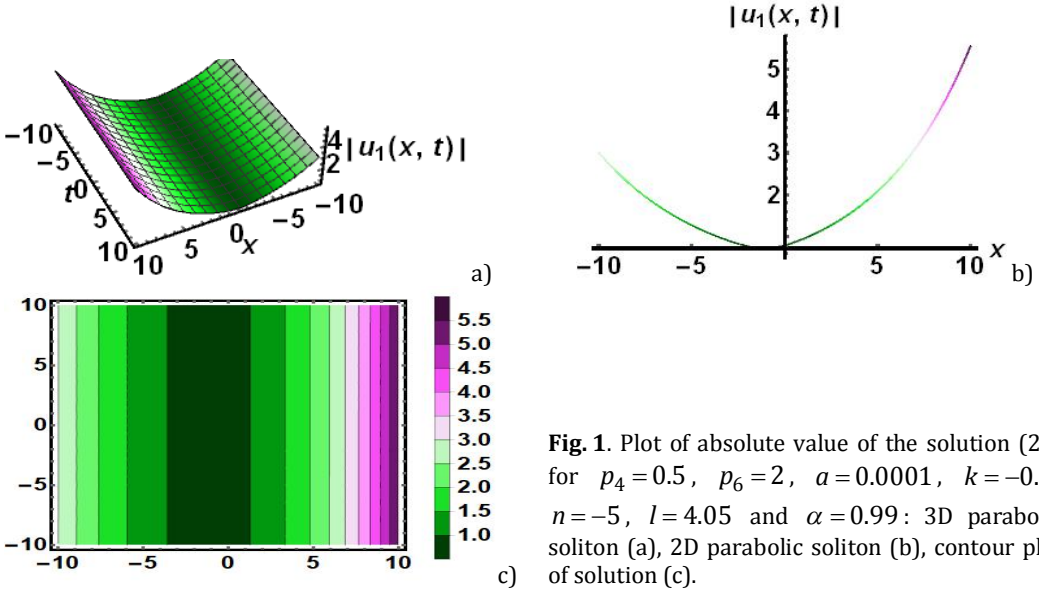

Fig. 1. Plot of absolute value of the solution (22) for $p_4 = 0.5$, $p_6 = 2$, $a = 0.0001$, $k = -0.8$, $n = -5$, $l = 4.05$ and $\alpha = 0.99$: 3D parabolic soliton (a), 2D parabolic soliton (b), contour plot of solution (c).

The absolute plot of solution (22) gives a parabolic-shaped soliton for the definite values of $p_4 = 0.5$, $p_6 = 2$, $a = 0.0001$, $k = -0.8$, $n = -5$, $l = 4.05$, and $\alpha = 0.99$. The 3D and contour graphs are drawn within the interval $-10 \le x$, $t \le 10$, as shown in Fig. 1a and Fig. 1c.

For $t=2$, the 2D plot is represented in Fig. 1b. For $n=0.25$ and $n=1.4$, singular and bright solitons are obtained for the modulus of solution (22) in the same interval, while the other remaining parameters are the same. The 3D plot, 2D plot for $t=2$, and contour plots are illustrated in Fig. 2 and Fig. 3. A bell-shaped soliton is a localized and stable wave with a smooth, single-peaked profile. It preserves its shape and speed during propagation and even after interacting with other solitons. Such solitons commonly appear in nonlinear systems, such as the nonlinear Schrödinger equation, and are used in optical fiber communication, fluid dynamics, and plasma physics for dispersion-free transport of energy or information. The modulus plot of the solution (22) represents the singular periodic wave shape soliton for the values $p_4=0.5$, $p_6=2$, $a=0.0001$, $k=-0.5$, $n=0.55$, $l=4.05$, and $\alpha=0.5$ within the interval $-30\le x\le 20$, $-10\le t\le 10$. The 3D, contour, and 2D plots for $t=2$ as shown in Fig. 4. Further, the solution (22) gives the peakon soliton in the interval $-6\le x\le 6$, $-10\le t\le 10$ for $k=-0.8$, $n=1.4$, and $\alpha=0.7$, while the other variables are identical. The contour, 3D, and 2D plots are depicted in Fig. 5. A peakon is a solitary wave with a sharp and pointed crest. Its profile is continuous but not differentiable at the peak, and it preserves its shape and speed during propagation. Peakons are useful for modeling shallow-water waves and other physical phenomena with sharp localized structures. A breather-type soliton is attained from $\mathrm{Re}(u_1(x,t))$ for definite values of $p_4=0.5$, $p_6=2.2$, $a=0.66$, $k=-0.8$, $n=0.45$, $l=2$, and $\alpha=0.47$ in the interval $0\le x$, $t\le 10$, which is shown in Fig. 6. A breather-type soliton refers to a wave pattern that combines the features of solitons and periodic waves. It behaves like a soliton because it keeps its shape and stability during propagation. It is a stable, localized wave that carries a repeating structure, placing it between a pure soliton and a fully periodic waveform. Further, for $p_4=p_6=-40$, $a=-0.001$, $k=0.8$, $n=1$, $l=-9.4$, and $\alpha=0.987$, the real part of the solution (22) gives the anti-bell-shaped soliton. The 3D and 2D plots for $t=0$ are shown in Fig. 7.

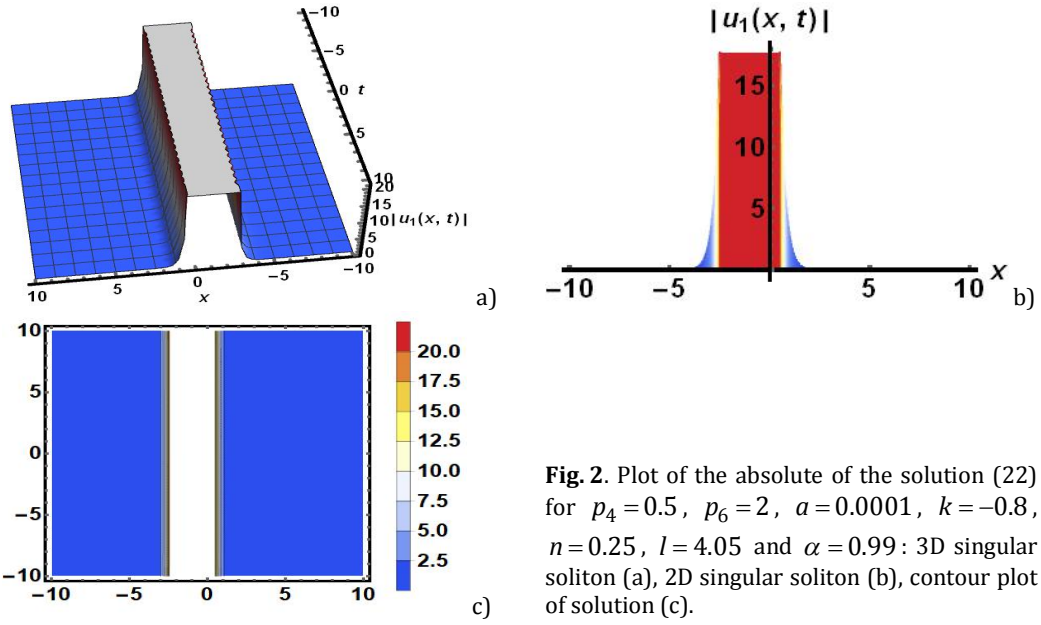

Fig. 2. Plot of the absolute of the solution (22) for $p_4=0.5$, $p_6=2$, $a=0.0001$, $k=-0.8$, $n=0.25$, $l=4.05$ and $\alpha=0.99$: 3D singular soliton (a), 2D singular soliton (b), contour plot of solution (c).

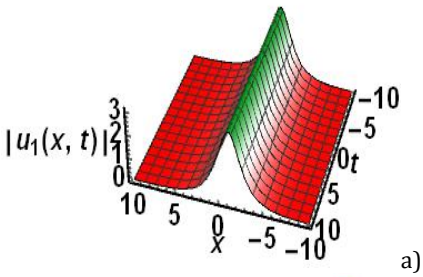

a)

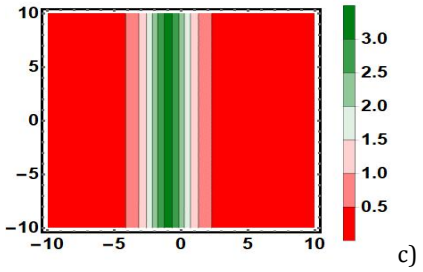

c)

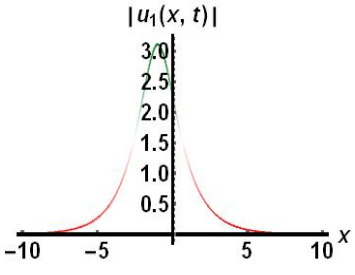

b)

Fig. 3. Plot of the absolute of the solution (22) for $p_4 = 0.5$, $p_6 = 2$, $a = 0.0001$, $k = -0.8$, $n = 1.4$, $l = 4.05$ and $\alpha = 0.99$: 3D bright soliton (a), 2D bright soliton (b), contour plot of solution (c).

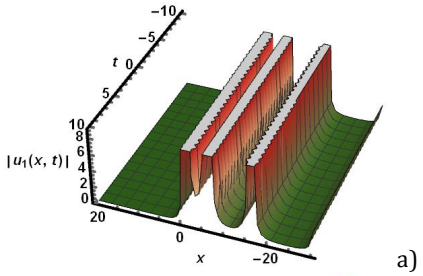

a)

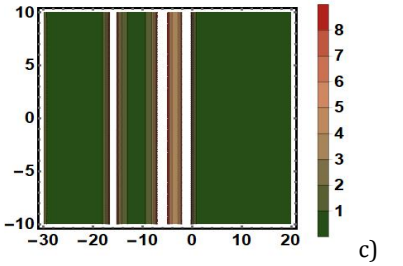

c)

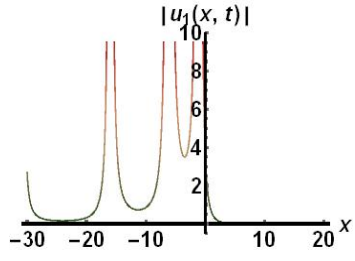

b)

Fig. 4. Plot of the absolute of the solution (22) for $p_4 = 0.5$, $p_6 = 2$, $a = 0.0001$, $k = -0.5$, $n = 0.55$, $l = 4.05$, and $\alpha = 0.5$: 3D singular periodic soliton (a), 2D singular periodic soliton (b), contour plot of solution (c).

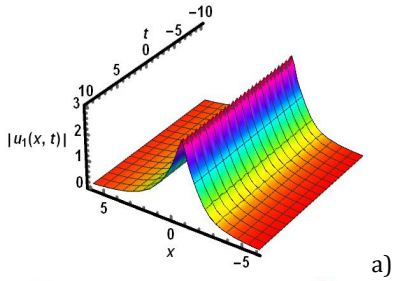

a)

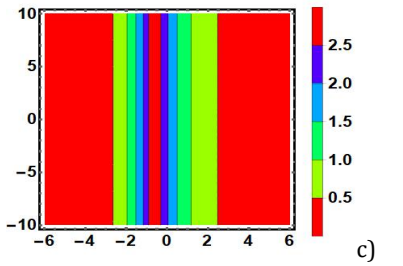

c)

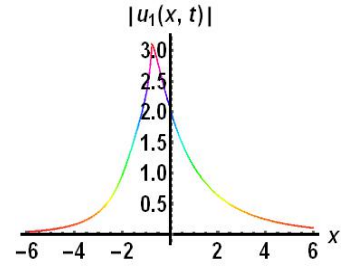

b)

Fig. 5. Plot of the absolute of the solution (22) for $p_4 = 0.5$, $p_6 = 2$, $a = 0.0001$, $k = -0.8$, $n = 1.4$, $l = 4.05$, and $\alpha = 0.7$: 3D peakon soliton (a), 2D peakon soliton (b), contour plot of solution (c).

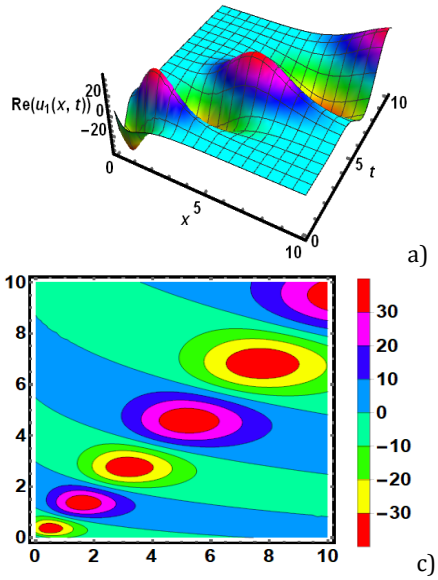

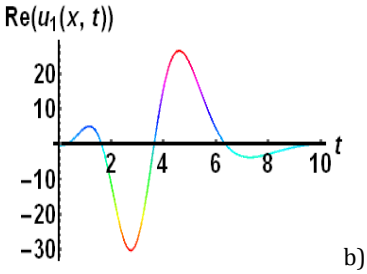

Fig. 6. Plot of $\mathrm{Re}(u_1(x,t))$ for $p_4=0.5$, $p_6=2.2$, $a=0.66$, $k=-0.8$, $n=0.45$, $l=2$, and $\alpha=0.47$: 3D breather-type soliton (a), 2D breather-type soliton (b), contour plot of Re($u_1(x,t)$) (c).

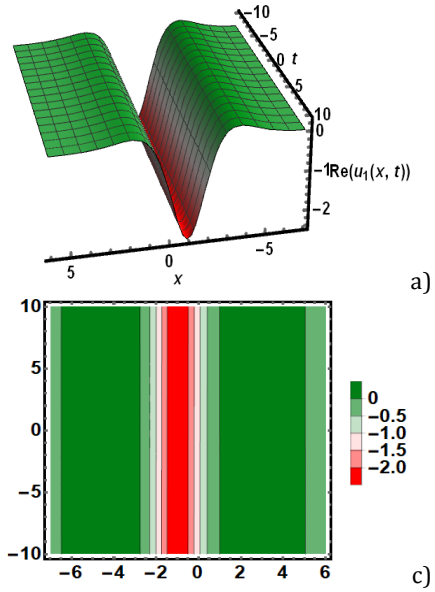

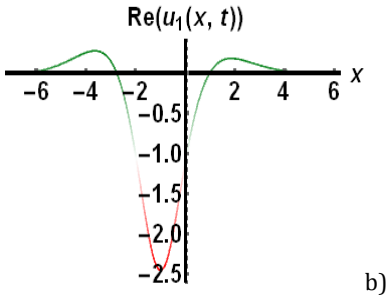

Fig. 7. Plot of $\mathrm{Re}(u_1(x,t))$ $p_4=p_6=-40$, $a=-0.001$, $k=0.8$, $n=1$, $l=-9.4$, and $\alpha=0.987$: 3D anti-bell-shaped soliton (a), 2D anti-bell-shaped soliton (b), contour plot of Re($u_1(x,t)$) (c).

The modulus plot of (24) represents the anti-kink-shaped soliton in the interval $-10\le x$, $t\le 10$ for certain values of $p_4=p_6=6$, $a=0.2$, $k=1.2$, $n=0.35$, $l=1$, and $\alpha=0.9999$. In Figs. 8a and 8c, 3D and contour plots are drawn. Also, for $t=0$, the 2D plot is depicted in Fig. 8b. An anti-kink-shaped soliton is a local wave that connects two different stable states with a smooth, monotonic profile that decays in the opposite direction of a kink soliton. It is useful for modeling domain walls, phase transitions, and signal propagation in optical and condensed-matter systems. $\mathrm{Re}(u_2(x,t))$ represents a periodic soliton for $p_4=p_6=-40$, $a=-0.0001$, $k=5.2$, $n=1$, $l=0.75$, and $\alpha=0.88$ with the interval $0\le x$, $t\le 10$. The 3D, 2D, and contour plots are depicted in Fig. 9 for $t=5$. A periodic soliton is a stable, repeating wave pattern that maintains its shape and amplitude over time while propagating through a nonlinear medium. The periodic solitons are used in optical communication, fluid dynamics, and plasma physics to model

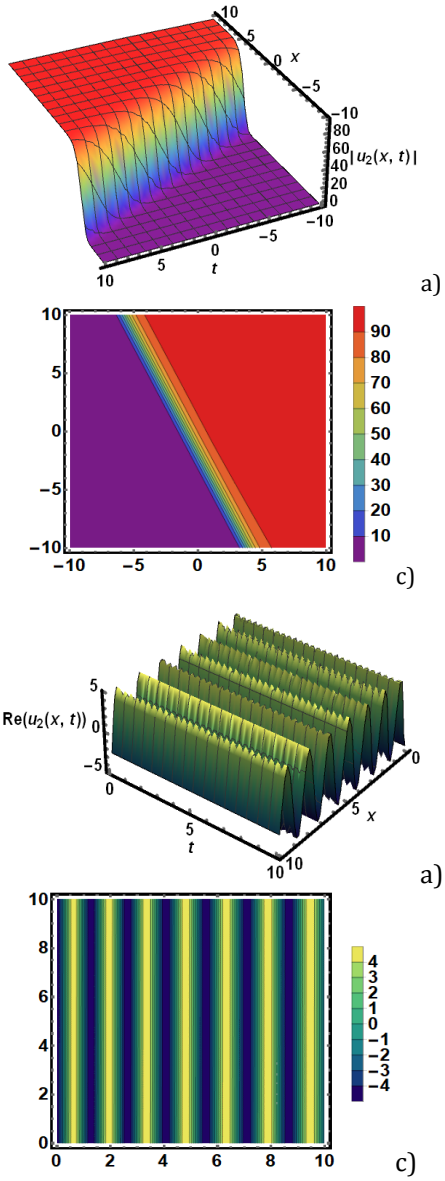

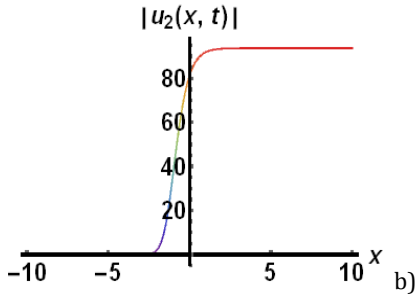

Fig. 8 Plot of solution (24) for $p_4 = p_6 = 6$, $a = 0.2$, $k = 1.2$, $n = 0.35$, $l = 1$, and $\alpha = 0.9999$: 3D anti-kink soliton (a), 2D anti-kink soliton (b), contour plot of (c).

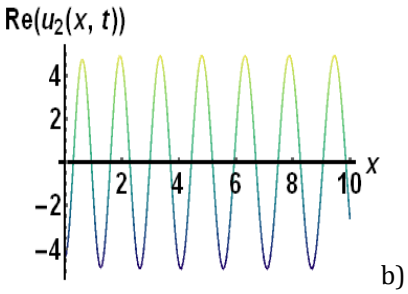

Fig. 9. Plot of solution (24) for $p_4 = p_6 = -40$, $a = -0.0001$, $k = 5.2$, $n = 1$, $l = 0.75$, and $\alpha = 0.88$: 3D periodic soliton (a), 2D periodic soliton (b), contour plot of $\mathrm{Re}(u_2(x,t))$ (c).

and control wave trains or recurring energy patterns. The $\mathrm{Im}(u_2(x,t))$ also represents the periodic soliton for $p_4 = 14$, $p_6 = 15$, $a = -4$, $k = -6.8$, $n = 1$, $l = 0.75$, and $\alpha = 0.88$ with the interval $0 \le x$, $t \le 10$. The 3D and 2D plots are depicted in Figs. 10a and 10b, and the density plot is depicted in 10c for $t = 12$. The modulus plot of solution (26) gives the peakon soliton for corresponding values of $p_4 = p_6 = 1.4$, $a = 0.001$, $k = -0.8$, $n = 5$, $l = 1$, and $\alpha = 0.69$ with the interval $-10 \le x$, $t \le 10$. In Fig. 11(a), a 3D plot, Fig. 11(b), a 2D plot for $t = 0$, and Fig. 11c, a contour plot, are presented. Further, for corresponding values of $p_4 = p_6 = 1.4$, $a = 0.5$, $k = -0.8$, $n = 1.4$, $l = 1$, and $\alpha = 0.999$, the modulus of solution (26) yields the kink soliton with the same interval. The 3D, 2D plot for $t = 0.5$ and the contour plot are displayed in Fig. 12. A thorough examination and characterization of kink-like optical solutions play a pivotal role in nonlinear photonics, optical communication technologies, and related disciplines that demand precise control over

light-intensity profiles. For certain values of $p_4 = p_6 = 8$, $a = 0.001$, $k = 1.5$, $n = 1$, $l = 1$, and $\alpha = 0.81$, the absolute value of solution (28) constructs the V-shaped soliton within the interval $-10 \le x$, $t \le 10$. The 3D plot, 2D plot for $t = 2$, and contour plot are displayed in Fig. 13.

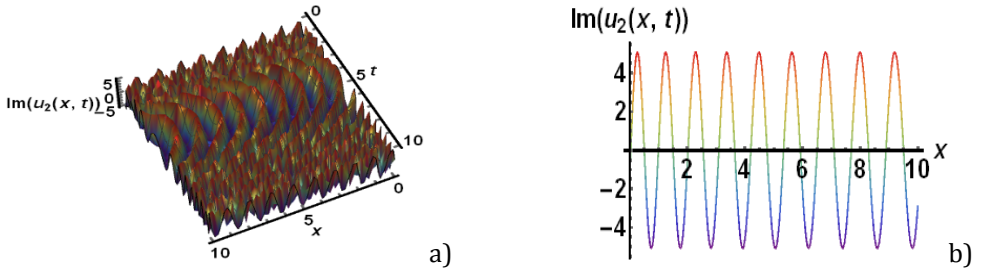

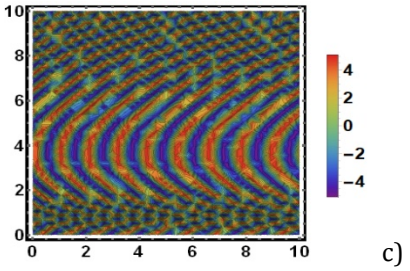

Fig. 10. Plot of imaginary part of solution (24) for $p_4 = 14$, $p_6 = 15$, $a = -4$, $k = -6.8$, $n = 1$, $l = 0.75$, and $\alpha = 0.88$: 3D periodic soliton (a), 2D periodic soliton (b), density plot of Im($u_2(x,t)$) (c).

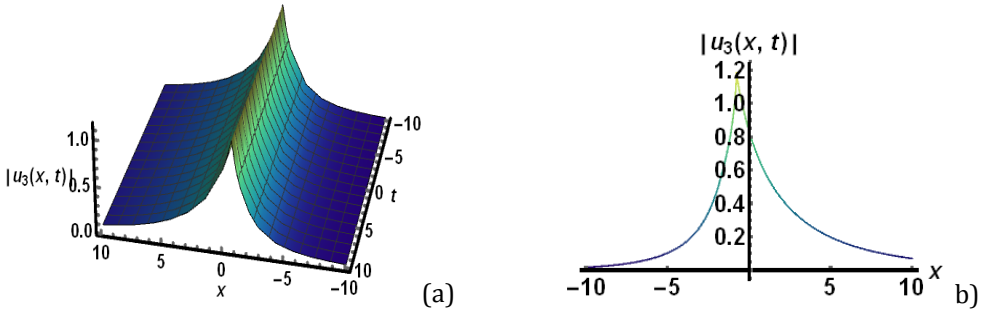

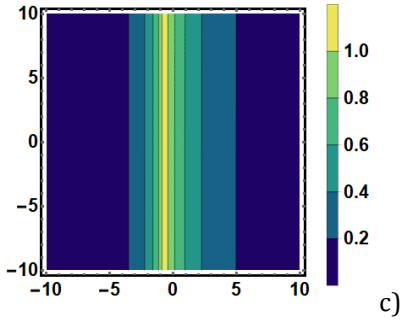

Fig. 11. Plot of $|u_3(x,t)|$ for $p_4 = p_6 = 1.4$, $a = 0.001$, $k = -0.8$, $n = 5$, $l = 1$ and $\alpha = 0.69$: 3D peakon soliton (a), 2D peakon soliton (b), contour plot of $|u_3(x,t)|$ (c).

An anti-peakon soliton is found from solution (30) for the values $p_4 = 2.2$, $p_6 = -6$, $a = 0.1$, $k = -0.2$, $n = 4.5$, $l = 2$, and $\alpha = 0.2$. 3D and 2D plots for $t = 0$, and a contour plot are depicted within the interval $-2 \le x \le 2$, $-10 \le t \le 10$ as shown in Fig. 14. The $\mathrm{Re}(u_5(x,t))$ yields the bright soliton for all values $p_4 = 1$, $p_6 = 3$, $a = 0.001$, $k = 0.6$, $n = 1$, $l = 2$, and $\alpha = 0.582$. The 3D, 2D for $t = 1$, and contour plots are displayed in Fig. 15 with the interval $-10 \le x \le 0$, $-10 \le t \le 10$. If we increase the fractional order from $\alpha = 0.582$ to $\alpha = 0.99$ without changing other parameters, then $\mathrm{Re}(u_5(x,t))$ gives the parabolic soliton in the

same interval. The graph displayed of 3D, contour, and 2D for $t=1$ is shown in Fig. 16. Further, $|u_5(x,t)|$ provided the bright soliton for all values of $p_4=7.4$, $p_6=8$, $a=-0.6$, $k=-1.6$, $n=6.3$, $l=1$, and $\alpha=0.95$. The 3D, 2D for $t=0$, and contour plots are displayed in Fig. 17 with the interval $-10\le x\le 0$, $-10\le t\le 10$. The solution (32) represents the anti-kink soliton for definite values of $p_4=5.8$, $p_6=5.2$, $a=0.001$, $k=2.2$, $n=0.65$, $l=1$ and $\alpha=0.99$ within the interval $-20\le x$, $t\le 20$. The 3D, 2D, and contour plots for $t=10$ are depicted in Fig. 18.

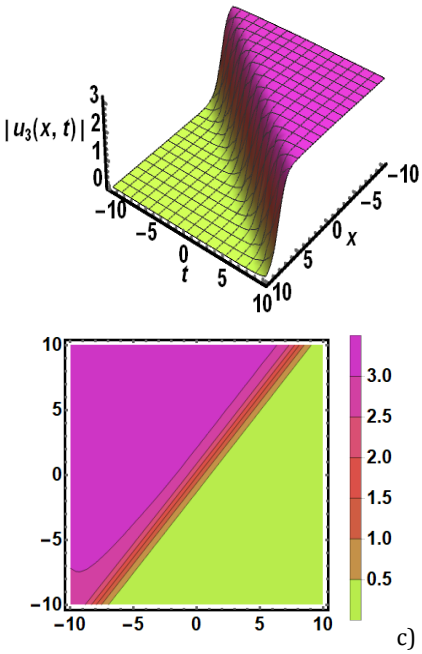

a) b) c)

Fig. 12. Plot of $|u_3(x,t)|$ for $p_4=p_6=1.4$, $a=0.5$, $k=-0.8$, $n=1.4$, $l=1$ and $\alpha=0.999$: 3D kink soliton (a), 2D kink soliton (b), contour plot of $|u_3(x,t)|$ (c).

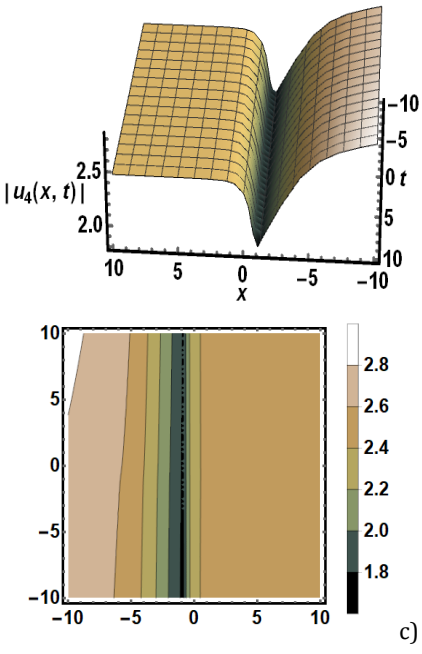

a) b) c)

Fig. 13. Plot of (28) for $p_4=p_6=8$, $a=0.001$, $k=1.5$, $n=1$, $l=1$, and $\alpha=0.81$: 3D V-shaped soliton (a), 2D V-shaped soliton (b), Contour plot of $|u_4(x,t)|$ (c).

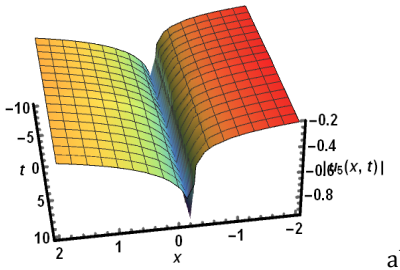

a)

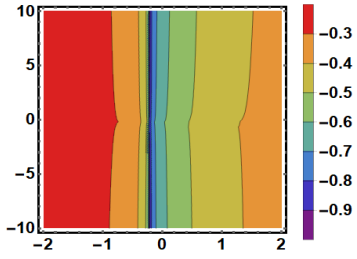

c)

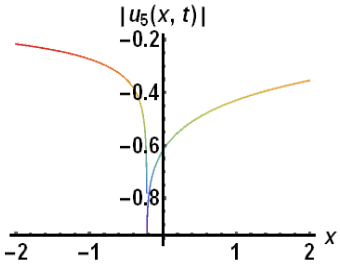

b)

Fig. 14. Plot of $|u_5(x,t)|$ for $p_4=2.2$, $p_6=-6$, $a=0.1$, $k=-0.2$, $n=4.5$, $l=2$ and $\alpha=0.2$: 3D plot of anti-peakon (a), 2D plot of anti-peakon (b), contour plot of anti-peakon (c).

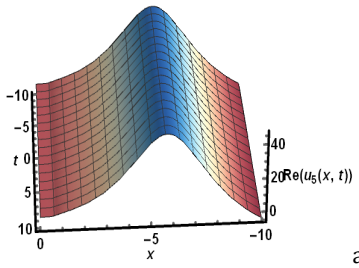

a)

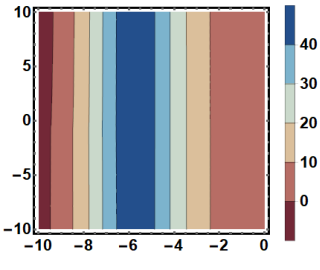

c)

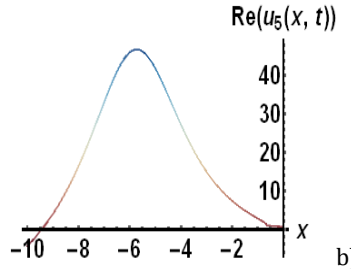

b)

Fig. 15. Plot of $\mathrm{Re}|u_5(x,t)|$ for $p_4=1$, $p_6=3$, $a=0.001$, $k=0.6$, $n=1$, $l=2$, and $\alpha=0.582$: 3D plot of bright soliton (a), 2D plot of bright soliton (b), contour plot of bright soliton (c).

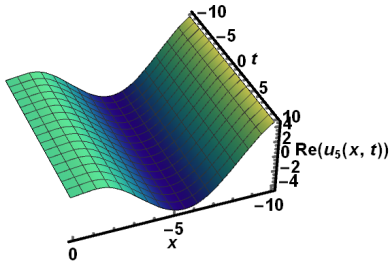

a)

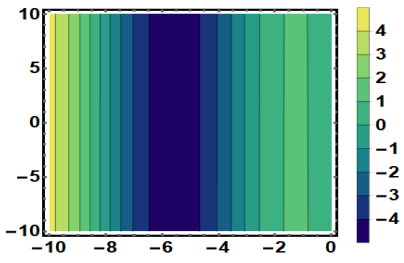

c)

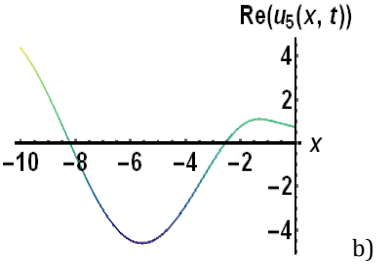

b)

Fig. 16. Plot of $\mathrm{Re}|u_5(x,t)|$ for $p_4=1$, $p_6=3$, $a=0.001$, $k=0.6$, $n=1$, $l=2$, and $\alpha=0.99$: 3D plot of parabolic soliton (a), 2D plot of parabolic soliton (b), contour plot of parabolic soliton (c).

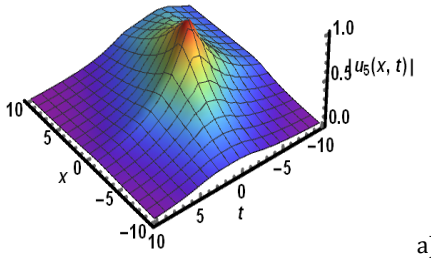

a)

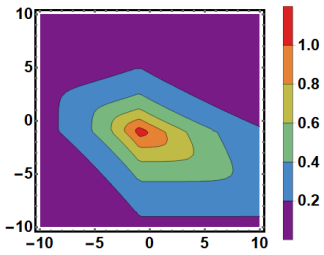

c)

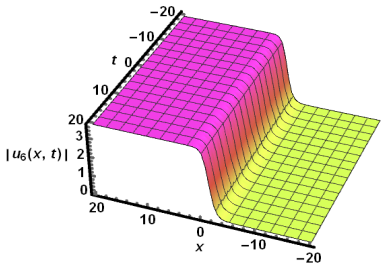

a)

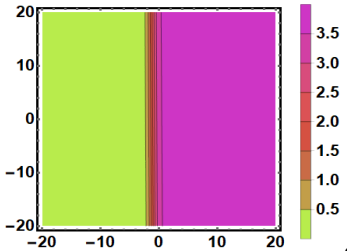

c)

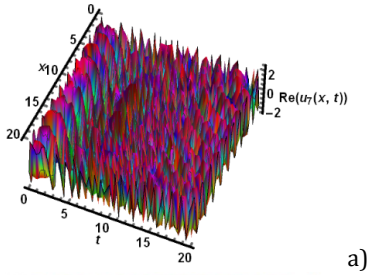

a)

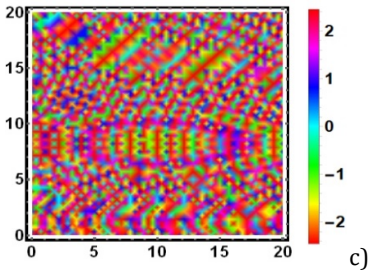

c)

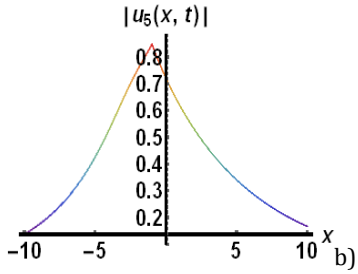

b)

Fig. 17. Plot of $|u_5(x,t)|$ for $p_4=7.4$, $p_6=8$, $a=-0.6$, $k=-1.6$, $n=6.3$, $l=1$, and $\alpha=0.95$: 3D plot of bright-type soliton (a), 2D plot of bright-type soliton (b), contour plot of bright-type soliton (c).

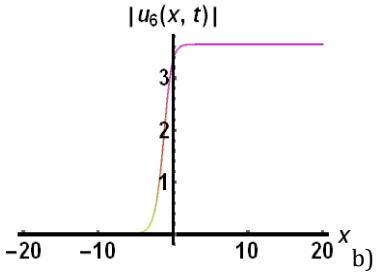

b)

Fig. 18. Plot of $|u_6(x,t)|$ for $p_4=5.8$, $p_6=5.2$, $a=0.001$, $k=2.2$, $n=0.65$, $l=1$ and $\alpha=0.99$: 3D plot of anti-kink (a), 2D plot of anti-kink (b), contour plot of anti-kink (c).

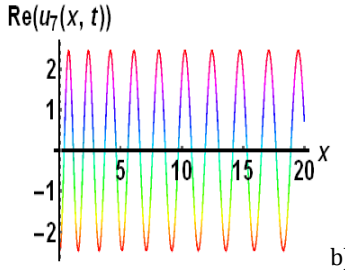

b)

Fig. 19. Plot of $\mathrm{Re}|u_7(x,t)|$ for $p_4=p_6=-40$, $a=-2$, $k=-4.6$, $n=1$, $l=2$, and $\alpha=0.994$: 3D plot of $\mathrm{Re}(u_7(x,\ t))$ (a), 2D plot of $\mathrm{Re}(u_7(x,\ t))$ (b), density plot of $\mathrm{Re}(u_7(x,t))$ (c).

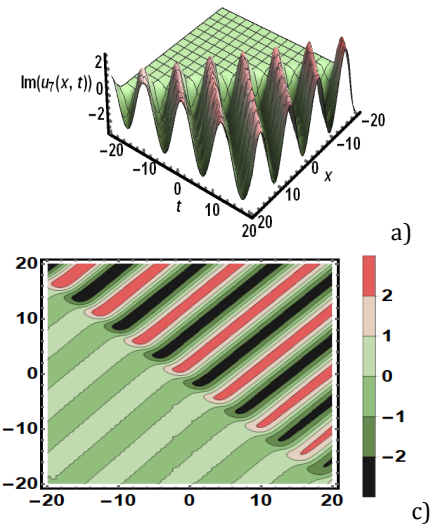

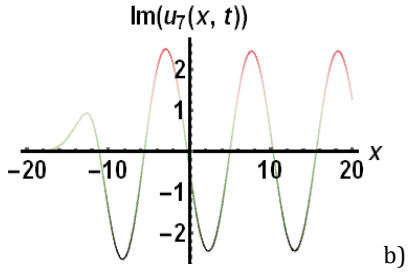

Fig. 20. Plot of $\mathrm{Im}\left|u_7(x,t)\right|$ for $p_4=p_6=2{,}2$, $a=0.9$, $k=0.6$, $n=1$, $l=2$, and $\alpha=0.808$: 3D plot of periodic-like soliton (a), 2D plot of periodic-like soliton (b), contour plot of $\mathrm{Im}(u_7(x,t))$ (c).

The real part of the solution $u_7(x,t)$ (solution (34)) yields a periodic soliton for the values of $p_4=p_6=-40$, $a=-2$, $k=-4.6$, $n=1$, $l=2$, and $\alpha=0.994$ within the intervals $0\le x$, $t\le 20$. The 3D and 2D plots for $t=10$ and the density plot are depicted in Figs. 19a, 19b, and 19c. Further, the imaginary portion of the solution $u_7(x,t)$ constructs periodic solitons for the corresponding values of $p_4=p_6=2.2$, $a=0.9$, $k=0.6$, $n=1$, $l=2$, and $\alpha=0.808$ within the same intervals. The 3D and 2D plots for $t=10$ and the contour plot are depicted in Figs. 20a, 20b, and 20c.

The graphical analysis clearly shows that the soliton profile is highly sensitive to some parameters. Small changes in the dispersion coefficient a significantly alter the width and spread of the soliton. The nonlinearity parameter n affects the strength of the nonlinear interaction, which changes the amplitude and sharpness of the soliton. The wavenumber k affects the oscillatory behavior and spatial properties of the soliton pattern. In addition, the fractional-order parameter α significantly affects the overall structure and evolution of the soliton solution. Changing α changes the propagation behavior and profile shape of the soliton. As these parameters change, the soliton's height, width, and localization also change. Therefore, the combined effects of a, n, k, and α play a significant role in determining the structure and behavior of the soliton solution.

5.2. The time-space fractional higher-order NLS equation

The physical representations of the acquired solutions of the higher-order fractional time-space NLS equation for various parameters are discussed in this section. We have divided the solutions into three parts and illustrated them, such as real parts, imaginary parts, and modulus, to understand and demonstrate the physical significance of the obtained solutions. Solution (45) ($\left|v_1(x,t)\right|$) gives the anti-kink soliton for $a=0.4$, $k=0.9$, $n=1$, and $\gamma=0.8$ with fractional order $\alpha=0.999$ within the intervals $-20\le x$, $t\le 20$ and is shown in Fig. 21a, a 3D plot, and Fig. 21b, a 2D plot displayed for $t=0$. Also, in Fig. 21c, a contour plot is portrayed. The cuspon soliton is depicted from the real portion of the solution $v_1(x,t)$ for $a=-0.001$, $k=0.1$, $n=-0.8$, $\gamma=0.6$, and $\alpha=0.044$ throughout the intervals $-10\le x$, $t\le 10$ and shown in Fig. 22. Further, Fig. 22b shows a 2D plot for t=5. Keeping a, n, and γ as constants, the

real portion of the solution $v_1(x,t)$ constructs the anti-cuspon soliton for $k=0.3$ and $\alpha=0.01$ with the same intervals as shown in Fig. 23a: 3D plot; Fig. 23b: 2D plot for t=5 ; and Fig. 23c: contour plot. Again, keeping a and γ as constant, the real portion of the solution $v_1(x,t)$ constructs the parabolic soliton for $k=1.4$, $n=3.4$, and $\alpha=0.222$ with the intervals $-10\le x\le -1$ and $-10\le t\le 10$ as shown in Fig. 24a: 3D plot; Fig. 24b: 2D plot for $t=-5$ and Fig. 24c: contour plot. $\mathrm{Re}(v_1(x,t))$ gives the periodic soliton for $a=-1.6$, $k=0.4$, $n=0.55$, $\gamma=0.6$, and $\alpha=0.99$. The 3D and contour graphs are drawn throughout the intervals $5\le x\le 60$ and $0\le t\le 20$. Also, the 2D graph for $x=-40$ is shown in Fig. 25. Further, for $a=-1.35$, $k=-40$, $n=5$, $\gamma=0.6$, and $\alpha=0.418$, the real part of the solution $v_1(x,t)$ represented the breather-type soliton within the intervals $0\le x$, $t\le 10$. 3D graph, 2D graph for $t=5$, and density graph as shown in Fig. 26. For all the values of $a=0.5$, $k=-0.8$, $n=8.6$, $\gamma=2.8$, $\alpha=0.988$ and in the intervals $-15\le x\le 10$, $-10\le t\le 10$, $\mathrm{Im}(v_1(x,t))$ yields the periodic soliton whose amplitude is initially low, but gradually increases. The 3D graph, 2D graph for $t=0.5$, and contour graph are demonstrated in Fig. 27.

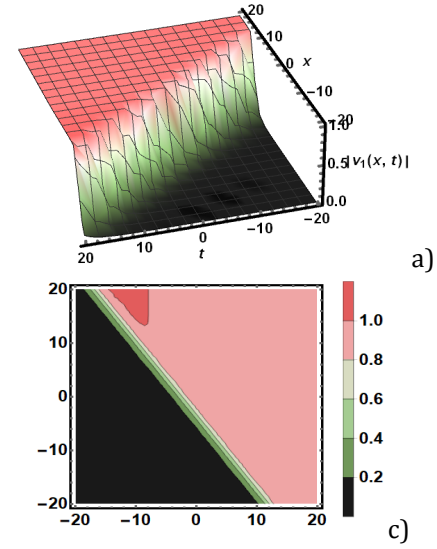

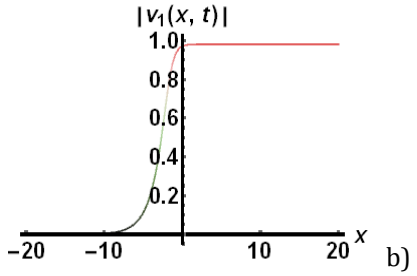

Fig. 21. Plot of $|v_1(x,t)|$ for $a=0.4$, $k=0.9$, $n=1$, and $\gamma=0.8$ with fractional order $\alpha=0.999$: 3D plot of anti-kink (a), 2D plot of anti-kink (b), contour plot of anti-kink(c).

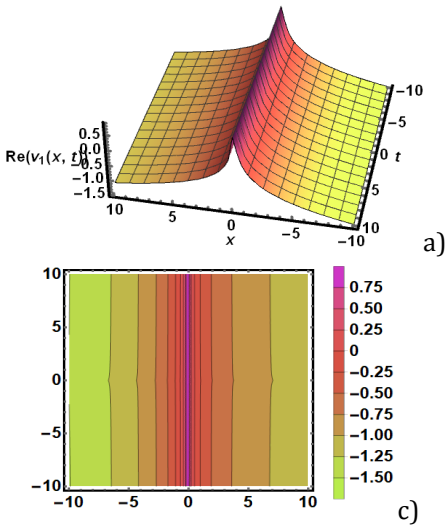

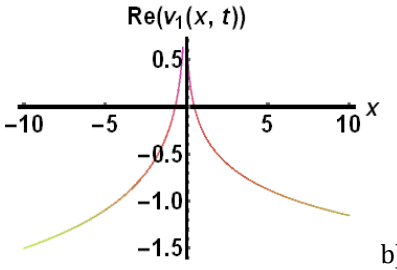

Fig. 22. Plot of $\mathrm{Re}(v_1(x,t))$ for $a=-0.001$, $k=0.1$, $n=-0.8$, $\gamma=0.6$, and $\alpha=0.044$: 3D plot of cuspon (a), 2D plot of cuspon (b), contour plot of cuspon (c).

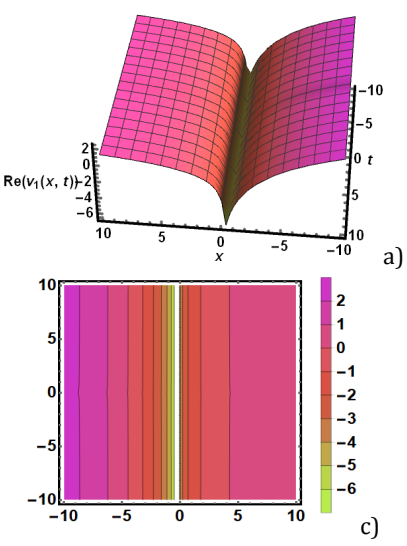

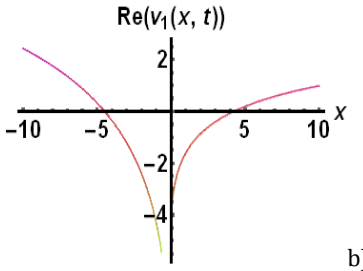

Fig. 23. Plot of $\mathrm{Re}(v_1(x,t))$ for $a=-0.001$, $k=0.3$, $n=-0.8$, $\gamma=0.6$, and $\alpha=0.01$: 3D plot of anti-cuspon (a), 2D plot of anti-cuspon (b), contour plot of anti-cuspon (c).

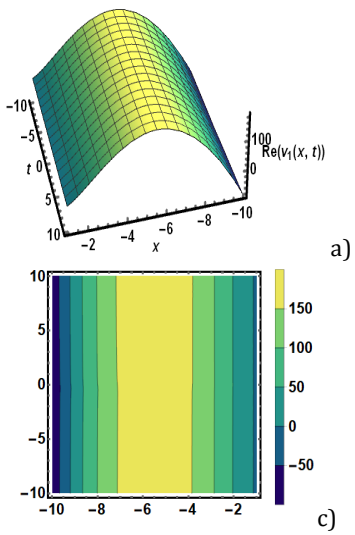

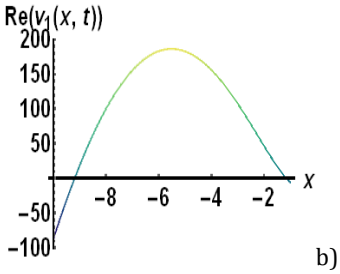

Fig. 24. Plot of $\mathrm{Re}(v_1(x,t))$ for $a=-0.001$, $k=1.4$, $n3.4$, $\gamma=0.6$, and $\alpha=0.222$: 3D plot of parabolic soliton (a), 2D plot of parabolic soliton (b), contour plot of parabolic soliton (c).

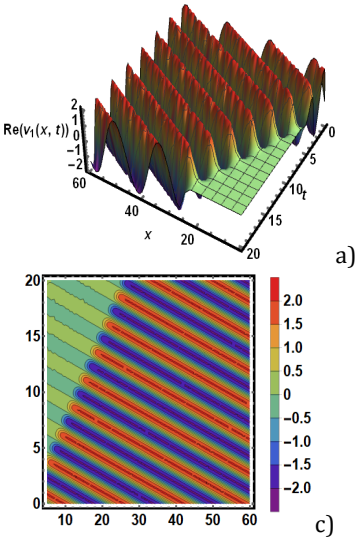

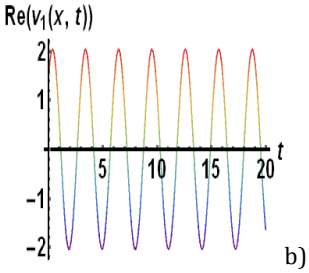

Fig. 25. Plot of $\mathrm{Re}(v_1(x,t))$ for $a=-1.6$, $k=0.4$, $n=0.55$, $\gamma=0.6$, and $\alpha=0.99$: 3D plot of periodic soliton (a), 2D plot of periodic soliton (b), contour plot of periodic soliton (c).

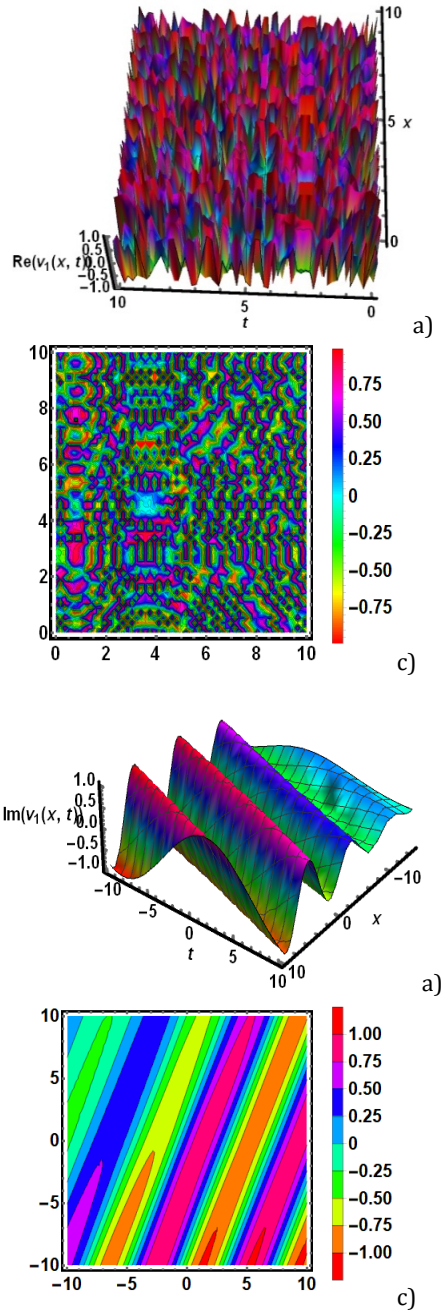

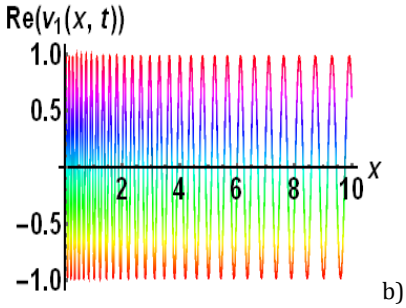

Fig. 26. Plot of $\mathrm{Re}(v_1(x,t))$ for $a=-1.35$, $k=-40$, $n=5$, $\gamma=0.6$, and $\alpha=0.418$: 3D plot of breather-type soliton (a), 2D plot of breather-type soliton (b), density plot of Re(v1(x,t)) (c).

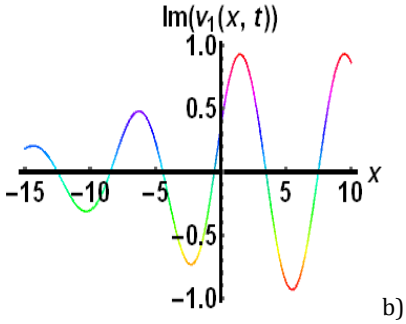

Fig. 27. Plot of $\mathrm{Im}(v_1(x,t))$ for $a=0.5$, $k=-0.8$, $n=8.6$, $\gamma=2.8$, $\alpha=0.988$: 3D plot of periodic-like soliton (a), 2D plot of periodic-like soliton (b), contour plot of Im(v1(x,t)) (c).

Solution (47) ($|v_2(x,t)|$) represents the sharp bell-shaped soliton within the intervals $-2\le x\le 2$ and $-20\le t\le 20$ for values of the parameters $a=-3$, $k=1.4$, $n=9.55$, $\gamma=5$, and $\alpha=0.98$. For $x=0.5$, the 2D and 3D plots are shown in Fig. 28b and 28a, respectively. Also, Fig. 28c represented the contour plot. Keeping the value of a, n, fractional order α and γ as constant, the modulus of the solution $|v_2(x,t)|$ constructs the singular bright soliton for $k=2$ with the same intervals as shown in Fig. 29a: 3D plot; Fig. 29b: 2D plot for $x=0.5$, and Fig. 29c: contour plot. For $a=-1.8$, $k=0.44$, $n=5$, $\gamma=2.8$ and fractional $\alpha=0.888$,

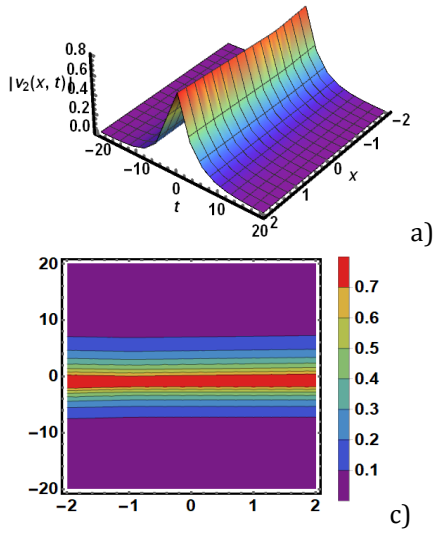

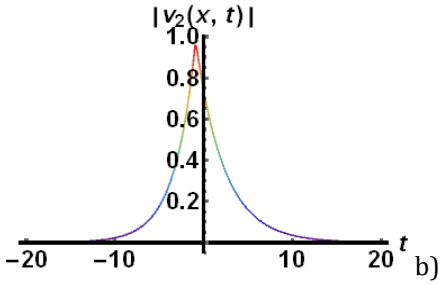

Fig. 28. Plot of $|v_2(x,t)|$ for $a=-3$, $k=1.4$, $n=9.55$, $\gamma=5$, $\alpha=0.98$: 3D sharped bell-shaped soliton (a), 2D sharped bell-shaped soliton (b), Contour plot of $|v_2(x,t)|$ (c).

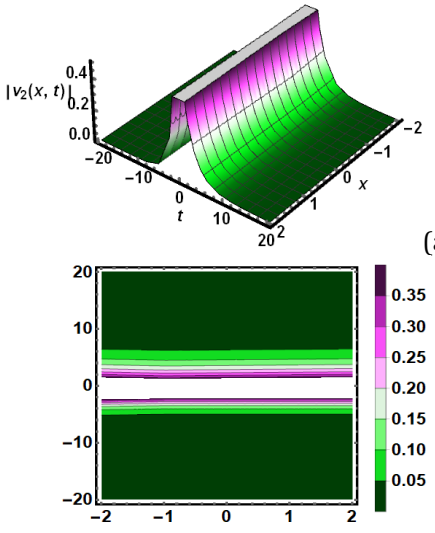

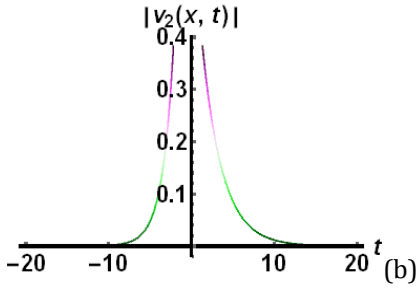

Fig. 29. Modulus plot of $|v_2(x,t)|$ for $a=-3$, $k=2$, $n=9.55$, $\gamma=5$, $\alpha=0.98$: 3D singular bright soliton (a), 2D singular bright soliton (b), contour plot of $|v_2(x,t)|$ (c).

$\mathrm{Re}(v_2(x,t))$ gives the periodic-like soliton as depicted in Fig. 30a: 3D, graph; Fig. 30(c): contour graph and Fig. 30b: 2D graph for $x=0$ with the intervals $-2\le x\le 2$, $-30\le t\le 30$. Further, for $a=-0.1$, $k=-1.6$, $n=7$, $\gamma=2$, and fractional $\alpha=0.99$, $\mathrm{Im}(v_2(x,t))$ gives the periodic-like soliton as depicted in Fig. 31a: 3D graph; Fig. 31c: contour graph and Fig. 31b: 2D graph for $t=0.5$ within the intervals $-20\le x, t\le 20$. From the 2D graph in Fig. 31b, we see that the periodic-like soliton's amplitude starts minimal and incrementally amplifies over time, ultimately reaching a predetermined value. Bell-shaped solitons commonly arise in shallow-water wave dynamics and optical pulse propagation, whereas cuspon structures are typically linked to plasma and fluid phenomena. Parabolic and V-type solitons exhibit shock-like characteristics, while breather solutions describe spatially localized oscillatory behavior in plasmas or fluid flows.

From the above analysis, it is evident that several parameters strongly affect the wave profile. In particular, the dispersion coefficient a, the nonlinearity power n, the wave

number k, and the fractional-order α significantly affect the amplitude, width, and overall shape of the soliton. Variations of these parameters change how the soliton forms evolve over space and time. This performance indicates that these parameters play a fundamental role in controlling the soliton's modulation and propagation dynamics.

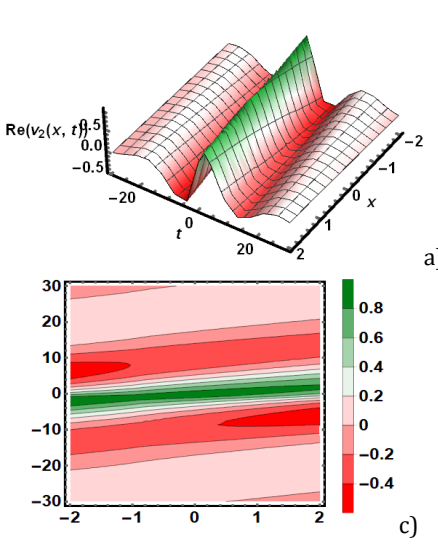

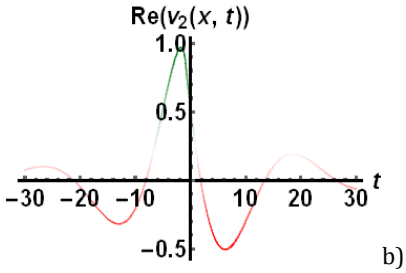

Fig. 30. Plot of $\mathrm{Re}(v_2(x,t))$ for $a=-1.8$, $k=0.44$, $n=5$, $\gamma=2.8$ and $\alpha=0.888$: 3D periodic-like soliton (a), 2D periodic-like soliton (b), contour plot of Re(v2(x,t)) (c).

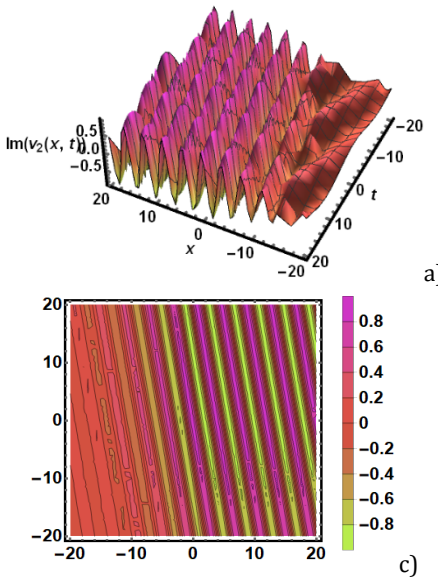

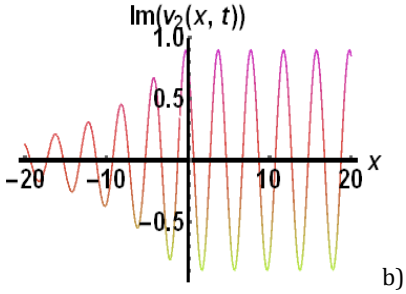

Fig. 31. Plot of $\mathrm{Im}(v_2(x,t))$ for $a=-0.1$, $k=-1.6$, $n=7$, $\gamma=2$, and $\alpha=0.99$: 3D periodic-like soliton (a), 2D periodic-like soliton (b), contour plot of Im(v2(x,t)) (c).

6. Discussion

In this section, we examine the differences between the integer-order and fractional-order models (1) and (2). Gepreel et al. [28] derived dark, bright, and singular soliton solutions for the classical NLS equation (1) incorporating Kudryashov's generalized refractive index. Furthermore, Kudryashov [29] obtained periodic-like, bell-shaped, and dark soliton solutions for the classical NLS-type equation (2). In the present study, we develop a wider spectrum of soliton structures, including periodic, parabolic, singular-periodic, kink, anti-kink, bright, dark, bright-dark, cusp, anti-cusp, peakon, anti-peakon, breather, and V-shaped solitons arising from the fractional versions of these equations for several values of the fractional operator. By

highlighting the broader significance of the results, we investigate the effects of both the fractional-order parameter and the temporal parameters, demonstrating their critical influence on the resulting optical solutions. This analysis provides meaningful insights into the intricate behavior inherent in present-time fractional models. Compared with classical nonlinear Schrödinger equations, the considered fractional models exhibit greater flexibility, stronger nonlinearity, novel soliton structures, and improved predictive performance.

We compare the solutions obtained through the sine-Gordon expansion method with those reported in the literature using the new Kudryashov approach and the Bernoulli equation approach. This comparison highlights similarities and differences in solution structures, complexity, and physical relevance. It also demonstrates the effectiveness and broader solution capability of the sine-Gordon expansion method. A comparative study is presented in Table 2.

Table 2. Comparison study diagram.

Assessor	Studied model	Applied approach	Obtained solutions
Murad *et al.* [31]	The space-time fractional NLS equation with the Kudryashov arbitrary refractive index	The new Kudryashov approach	Several types of soliton such as bell-shaped, bright, and mixed dark-bright solitons
Murad and Arnous [32]	The space-time fractional NLS equation with the Kudryashov arbitrary refractive index	The Kudryashov method and the enhanced modified tanh expansion method	The bell-shaped, bright, mixed dark-bright and kink-type solitons
Murad *et al.* [33]	The space-time fractional NLS equation with the Kudryashov arbitrary refractive index	The Bernoulli equation approach and the new Kudryashov approach	Periodic soliton, dark, bright, singular, bell-shaped, and mixed dark-bright solitons
The present study	The space-time fractional NLS equation with the Kudryashov arbitrary refractive index	The sine-Gordon expansion approach	Several types of soliton such as periodic, singular periodic, parabolic, kink, anti-kink, bright soliton, dark soliton, mixed bright-dark soliton, cusp, anti-cusp soliton, peakon, anti-peakon soliton, breather soliton, and V-shaped solitons, etc.

The comparative analysis shows that the new Kudryashov approach and the Bernoulli equation approach are simple and computationally efficient, but it is limited in describing complex nonlinear wave structures. On the other hand, although the sine-Gordon expansion

method requires more algebraic computation, it is more effective at generating a wider range of solution types. This confirms the robustness and wider applicability of the sine-Gordon expansion approach for fractional nonlinear evolution models.

7. Linear stability analysis

In this section, we aim to delineate the stability analysis of the proposed model through a straightforward technique, named the linear stability approach. Assume that, U_0 is an equilibrium solution for Eq. (1). We introduce a perturbed wave solution of amplitude $U(x,t)$ with a view to inspecting the stability under the action of a perturbed force. The perturbed wave solution of Eq. (1) is

$$u(x,t)=\alpha U(x,t)+U_0\,. \tag{48}$$

Substituting the perturbed solution into Eq. (1) and linearizing, we obtain

$$\mathrm{i}\alpha D_t^{\beta}U+a\alpha \mathrm{D}_{xx}^{2\beta}U+\alpha p_1 UU_0{}^n+\alpha p_2 UU_0{}^{2n}+\alpha p_3 UU_0{}^{3n}+\alpha p_4 UU_0{}^{4n}=0\,, \tag{49}$$

Being a linear differential equation, the solution of Eq. (49) can be described as:

$$U(x,t)=\exp\left[i\left(\frac{k_0}{\beta}\left(x+\frac{1}{\Gamma(\beta)}\right)^{\beta}-\frac{v_0}{\beta}\left(t+\frac{1}{\Gamma(\beta)}\right)^{\beta}\right)\right],$$

where k_0 and v_0 stand for wave number and velocity of the perturbed. Placing $U(x,t)$ into Eq. (49), we obtain the perturbed velocity as:

$$v_0=-\left(p_1U_0^n+p_2U_0^{2n}+p_3U_0^{3n}+p_4U_0^{4n}-ak_0^2\right).$$

Since $\left|U(x,t)\right|=1$, the stability of the perturbed system depends on the velocity v_0. The velocity of the perturbed solution portrays a parabolic stable profile for the chosen values $p_1=-3$, $p_2=-4$, $p_3=-7$, $p_4=-3$, $U_0=4$, $n=3$, and, $a=2$ as depicted in Fig. 32(a). Here, $(v_0,k_0)=(v_0,0)$ is the equilibrium point for the given model, and small perturbations around the equilibrium tend to remain bounded, indicating stable behavior of the system. On the other hand, if we choose $a<0$, the system exhibits an unstable profile as shown in Fig. 32(b). In this case, small perturbations move away from the equilibrium point, which leads to unstable behavior.

Thus, the wave solution remains bounded because its amplitude is constant, but the model's overall stability depends on the parameter a. The system is stable when $a>0$ and unstable for $a<0$, while $a=0$ corresponds to a neutral case where the velocity becomes constant.

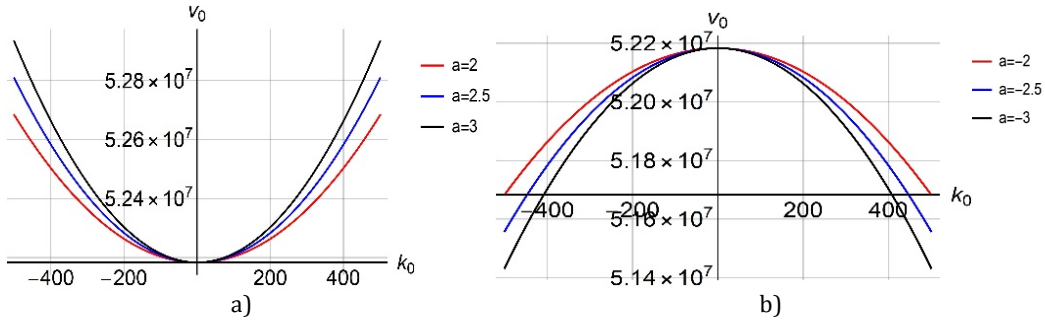

Fig. 32. Velocity profile of the perturbed wave solution: stable profile for $a>0$ (a), unstable profile for $a<0$ (b).

8. Conclusions

In this article, we investigate optical soliton solutions of two variants of the NLS equation incorporating Kudryashov's arbitrary refractive index and a β-fractional-order derivative. The sine-Gordon expansion approach is used to derive novel, stable, and physically meaningful optical soliton solutions under appropriate constraints. A wide class of new soliton structures for the time-fractional NLS model is obtained, and all solutions are shown to satisfy the governing equations. The resulting solitons have potential relevance across several research areas, including nonlinear optics, condensed matter physics, water wave theory, and biophysics. Symbolic computations are carried out using Maple, while Wolfram Mathematica is used to visualize the solutions through three-dimensional, two-dimensional, density, and contour plots. These solutions reveal a wide variety of wave structures, including periodic, parabolic, singular-periodic, kink, anti-kink, bright, dark, cusp, peakon, breather, cusp-like, and V-shaped solitons. This study highlights the effectiveness and adaptability of the suggested approach, suggesting its potential applications to other fractional and integer-order nonlinear models. The results may enhance the theoretical and conceptual understanding of time-fractional dynamical systems and open new directions for further speculative and practical studies of time-fractional dynamics.

Acknowledgement and funding. This research has been funded by the Scientific Research Deanship at the University of Ha'il, Saudi Arabia through project number RG-25050.

Authorship contribution statement

Wael W Mohammed: Conceptualization, Resources, Funding acquisition, Writing-Review Editing. **Md. Tipu Sultan**: Methodology, Investigation, Writing-Original Draft. **Mohamed S Algolam**: Software, Data Curation, Visualization, Writing-Review Editing. **M. Ali Akbar**: Project administration, Supervision, Writing-Review Editing. **Rabeb Sidaoui**: Formal Analysis, Validation, Writing-Review Editing.

Declaration of competing interest. The authors declare that they have no known competing financial interests or personal relationships that could have appeared to influence the work reported in this paper.

Data availability. All data generated or analysed during this study are included in this article.

References

1. Murad, M. A. S. (2023). New optical soliton solutions for time-fractional Kudryashov's equation in optical fiber. *Optik, 283*, 170897.
2. Zhang, G., Li, W., Yu, M., Huang, H., Wang, Y., Han, Z., Shi, K., Ma, L., Yu, Z., Zhu, X., Peng, Z., Xu, Y., Li, X., Hu, S., He, J., Li, D., Xi, Y., Lan, H., Xu, L., Tang, M., Xiao, M. (2023). Electric-field-driven printed 3D highly ordered microstructure with cell feature size promotes the maturation of engineered cardiac tissues. *Advanced Science*, *10*(11), 2206264.
3. Murad, M. A. S., Hamasalh, F. K., & Ismael, H. F. (2024). Time-fractional Chen–Lee–Liu equation: various optical solutions arising in optical fiber. *Journal of Nonlinear Optical Physics & Materials*, *33*(06), 2350061.
4. Liao, L., Guo, Z., Gao, Q., Wang, Y., Yu, F., Zhao, Q., Maybank, S. J., Liu, Z., Li, C., & Li, L. (2023). Color image recovery using generalized matrix completion over higher-order finite dimensional algebra. *Axioms*, *12*(10), 954.
5. Zulfiqar, H., Aashiq, A., Tariq, K. U., Ahmad, H., Almohsen, B., Aslam, M., Rehman, H. U. (2023). On the solitonic wave structures and stability analysis of the stochastic nonlinear Schrödinger equation with the impact of multiplicative noise. *Optik, 289*, 171250.
6. Ullah, N., Rehman, H. U., Imran, M. A., & Abdeljawad, T. (2020). Highly dispersive optical solitons with cubic law and cubic-quintic-septic law nonlinearities. *Results in Physics, 17*, 03021.
7. Kudryashov, N. A. (2019). A generalized model for description of propagation pulses in optical fiber. *Optik, 189*, 42–52.
8. Uddin, M. H., Khatun, M. A., Arefin, M. A., & Akbar, M. A. (2021). Abundant new exact solutions to the fractional nonlinear evolution equation via Riemann–Liouville derivative. *Alexandria Engineering Journal, 60*(6), 5183–5191.

9. Ali, E. E., Ennaceur, M., Mohammed, W. W., Algolam, M. S., & Ahmed, A. I. (2025). Investigation of new optical solutions for the fractional Schrödinger equation with time-dependent coefficients: Polynomial, random, trigonometric, and hyperbolic functions. *Fractal and Fractional, 9*, 142.
10. Aljoudi, S. (2021). Exact solutions of the fractional Sharma–Tasso–Olver equation and the fractional Bogoyavlenskii's breaking soliton equations. *Applied Mathematics and Computation, 405*, 126237.
11. Mohammed, W. W., Iqbal, N., Sidaoui, R., & Ali, E. E. (2025). Dynamical behavior of the fractional nonlinear Kadoma equation in plasma physics and optics. *Modern Physics Letters B, 39*, 2450434.
12. Korkmaz, O. E., Hepson, O., Hosseini, K., Rezazadeh, H., & Eslami, M. (2020). Sine-Gordon expansion method for exact solutions to conformable time fractional equations in RLW-class. *Journal of King Saud University – Science, 32*(1), 567–574.
13. Wang, K. J., & Shi, F. (2024). Non-singular complexiton, singular complexiton and complex N-soliton solutions of the new extended (3+1)-dimensional Boiti–Leon–Manna–Pempinelli equation. *Physica Scripta, 99*(3), 035251.
14. Wang, K. J. (2024). Multi-wave complexiton, interaction-wave and travelling wave solutions to the (2+1)-dimensional Boiti–Leon–Manna–Pempinelli equation for incompressible fluid. *Pramana – Journal of Physics, 98*(2), 47.
15. Wang, K. J. (2024). N-soliton, soliton molecules, Y-type soliton, periodic lump and other wave solutions of the reduced B-type Kadomtsev–Petviashvili equation. *European Physical Journal Plus, 139*(3), 275.
16. Islam, M. E., & Akbar, M. A. (2020). Stable wave solutions to the Landau–Ginzburg–Higgs equation and the modified equal width wave equation using the IBSEF method. *Arab Journal of Basic and Applied Sciences, 27*(1), 270–278.
17. Mohammed, W. W., Khatun, M. M., Algolam, M. S., Sidaoui, R., & Akbar, M. A. (2025). Analytical solitary wave solutions of fractional Tzitzéica equation using expansion approach. *Fractal and Fractional, 9*, 438.
18. Sofian, T. O., Ahmed, K. K., Ahmed, H. M., Mohammed, W. W., & Ghayad, M. S. (2025). Fractional derivative effects on soliton solutions of the (3+1)-D Kadomtsev–Petviashvili–Sawada–Kotera–Ramani model. *Contemporary Mathematics, 6*, 3846–5367.
19. Murad, M. A. S., Mahmood, S. S., Emadifar, H., Mohammed, W. W., & Ahmed, K. K. (2025). Optical soliton solution for dual-mode time-fractional nonlinear Schrödinger equation by generalized exponential rational function method. *Results in Engineering, 27*, 105591.
20. Alraddadi, F., Alsharif, F., Malik, S., Ahmad, H., Radwan, T., & Ahmed, K. K. (2024). Innovative soliton solutions for a (2+1)-dimensional generalized KdV equation using two effective approaches. *AIMS Mathematics, 9(*12), 34966–34980.
21. Alam, N., et al. (2025). Bifurcation analysis, chaotic behaviors, and explicit solutions for a fractional two-mode Nizhnik–Novikov–Veselov equation. *AIMS Mathematics, 10*(3), 4558–4578.
22. Murad, M. A. S, Mustafa, M. A., Younas, U., Emadifar, H., Khalifa, A. S., Mohammed W. W., Ahmed, K. K. (2025). Soliton solutions to the generalized derivative nonlinear Schrödinger equation under multiplicative white noise and conformable derivative. *Scientific Reports, 15*(1), 19599.
23. Samir, Ahmed, H. M., Emadifar, H., & Ahmed, K. K. (2025). Traveling and soliton waves in the extended (3+1)-dimensional Kadomtsev–Petviashvili equation. *Partial Differential Equations in Applied Mathematics, 14*, 101146.
24. Younas, U., Muhammad, J., Sulaiman, T. A., Ismael, H. F., Emadifar, H., Mohammed, W. W., Ahmed, K. K. (2025). Estevez–Mansfield–Clarkson equation: Investigation of breathers and solitary wave solutions. *Case Studies in Thermal Engineering, 74*, 106723.
25. Shehab, M. F., Ahmed, H. M., Boulaaras, S., Osman, M. S., & Ahmed, K. K. (2025). Impact of white noise on optical solitons in the stochastic fourth-order nonlinear Schrödinger equation. *Alexandria Engineering Journal, 127*, 1049–1063.
26. Ahmed, K. K., Ahmed, H. M., Shehab, M. F., Khalil, T. A., Emadifar, H., & Rabie, W. B. (2024). Characterizing stochastic soliton behavior in (3+1)-dimensional Schrödinger equation with cubic-quintic nonlinearity. *Physics Open, 21*, 100233.
27. Samir, Ahmed, K. K., Ahmed, H. M., Emadifar, H., & Rabie, W. B. (2024). Extraction of new soliton wave structures of generalized stochastic NLSE. *Physics Open, 21*, 100232.
28. Gepreel, K. A., Zayed, E. M. E., Alngar, M. E. M., Biswas, A., Guggilla, P., Khan, S., Yıldırım, Y., Alzahrani, A. K., Belic, M. R. (2021). Optical solitons with Kudryashov's arbitrary form of refractive index and generalized non-local nonlinearity. *Optik, 243*, 166723.
29. Kudryashov, N. A. (2020). Highly dispersive optical solitons with various polynomial nonlinearity law. *Chaos, Solitons & Fractals, 140*, 110202.
30. Kudryashov, N. A. (2020). Method for finding highly dispersive optical solitons of nonlinear differential equations. *Optik, 206*, 163550.
31. Murad, M. A. S. (2024). Optical solutions with Kudryashov's arbitrary type of generalized non-local nonlinearity. *Optical and Quantum Electronics, 56*(6), 999.
32. Murad, M. A. S., Arnous, A. H., Faridi, W. A., Iqbal, M., Nisar, K. S., & Kumar, S. (2024). Two algorithms for conformable time-fractional nonlinear Schrödinger equations. *Optical and Quantum Electronics, 56*(8), 1320.

33. Murad, M. A. S., Ismael, H. F., Sulaiman, T. A., & Bulut, H. (2024). Optical solutions of higher-order nonlinear Schrödinger equation via Kudryashov and Bernoulli approaches. *Optical and Quantum Electronics, 56*(1), 76.
34. Zayed, E.M., Shohib, R.M., Alngar, M.E., Biswas, A., Ekici, M., Khan, S., Alzahrani, A.K., & Belić, M.R. (2021). Optical solitons and conservation laws associated with Kudryashov's sextic power-law nonlinearity. *Ukrainian Journal of Physical Optics, 22*(1), 38–49.
35. Biswas, A., Ekici, M., Dakova, A., Khan, S., Moshokoa, S. P., Alshehri, H. M., Belic, M. R. (2021). Highly dispersive optical soliton perturbation with Kudryashov's sextic-power law nonlinear refractive index by semi-inverse variation. *Results in Physics, 27*, 104539.
36. Ozisik, M., Secer, A., Bayram, M., Cinar, M., Ozdemir, N., Esen, H., Onder, I. (2023). Optical soliton solutions of higher-order nonlinear Schrödinger equation with Kudryashov nonlinear refractive index. *Optik, 274*, 170548.
37. Xu, X. Z. (2023). Exact chirped solutions for the NLSE having Kudryashov's law with dual generalized non-local nonlinearity. *Optik, 287*, 171101.
38. Kayum, M. A., Ara, S., Osman, M. S., Akbar, M. A., & Gepreel, K. A. (2021). Broad-range stable soliton solutions of nonlinear equations in physics and gas dynamics. *Results in Physics, 20*, 103762.
39. Miller, K. S., & Ross, B. (1993). *An introduction to the fractional calculus and fractional differential equations*. Wiley.
40. Almeida, R. (2017). A Caputo fractional derivative of a function with respect to another function. *Communications in Nonlinear Science and Numerical Simulations, 44*, 460–481.
41. Khalil, R., Horani, M. A., Yousef, A., & Sababheh, M. (2014). A new definition of fractional derivative. *Journal of Computational and Applied Mathematics, 264*, 65–70.
42. Atangana, A., Baleanu, D., & Alsaedi, A. (2016). Analysis of time-fractional Hunter–Saxton equation. *Open Physics, 14*(1), 145–149.
43. Atangana, A., & Alqahtani, R. (2016). Modelling the spread of river blindness disease via the Caputo fractional derivative and beta-derivative. *Entropy, 18(*2), 40.
44. Ismael, H. F., Bulut, H., Baskonus, H. M., & Gao, W. (2021). Dynamical behaviors of the coupled Schrödinger–Boussinesq system with beta derivative. *AIMS Mathematics, 6*(7), 7909–7928.
45. Islam, M. N., Miah, M. M., Rahman, M. A., & Akbar, M. A. (2021). Closed-form wave solutions to space-time fractional nonlinear equations. *Partial Differential Equations in Applied Mathematics, 3*, 100024.

Mohammed, W. W., Sultan, Md. T., Algolam, M. S., Akbar, M. A., Sidaoui R. (2026). Analytical Study of Optical Solitons of the Space-Time Fractional Nonlinear Schrödinger Equations with Kudryashov's Refractive Index**.** *Ukrainian Journal of Physical Optics*, *27*(2), 02091 **–** 02123. doi: 10.3116/16091833/Ukr.J.Phys.Opt.2026.02091

Анотація. *У цій статті ми досліджуємо аналітичні оптичні солітони двох варіантів просторово-часового дробово-нелінійного рівняння Шредінгера, включаючи довільний показник заломлення Кудряшова. Моделі сформульовано з використанням β-дробової похідної, яка зберігає основні властивості класичного числення. Підхід розкладання синус-Гордона використовується для отримання точних та різноманітних солітонних розв'язків, включаючи комплексні, гіперболічні та тригонометричні форми. Отримані розв'язки описують широкий спектр солітонних структур, таких як яскраві, темні, каспонові, кінкові, антикінкові, параболічні та бризерні хвилі. Детальний параметричний аналіз показує, що коефіцієнти дробового порядку та нелінійні коефіцієнти суттєво впливають на амплітуду, ширину та динаміку поширення солітона. Графічне моделювання додатково підтверджує стабільність та багату структурну різноманітність розв'язків. Порівняльні результати демонструють, що підхід розкладання синус-Гордона є придатним, точним та широко застосовним. Він також забезпечує фізично значущі хвильові структури, які кращі за кілька існуючих методів, описаних у літературі. Отримані результати підкреслюють ефективність запропонованої структури для моделювання поширення нелінійних імпульсів у дробових оптичних волоконних системах та пов'язаних із цим застосувань у нелінійній оптиці.*

Ключові слова: *дробове нелінійне рівняння Шредінгера, β-дробова похідна, підхід розкладання синус-Гордона, оптичні солітони, показник заломлення Кудряшова*